Article

SOURCE DATA | TRANSPARENT PROCESS

THE EMBO JOURNAL

ATP-driven Rad50 conformations regulate DNA tethering, end resection, and ATM checkpoint signaling

Rajashree A Deshpande[1,†], Gareth J Williams[2,†], Oliver Limbo[3], R Scott Williams[4], Jeff Kuhnlein[1], Ji-Hoon Lee[1], Scott Classen[5], Grant Guenther[2], Paul Russell[3], John A Tainer[2,3,6,**] & Tanya T Paull[1,*]

Abstract

The Mre11-Rad50 complex is highly conserved, yet the mechanisms by which Rad50 ATP-driven states regulate the sensing, processing and signaling of DNA double-strand breaks are largely unknown. Here we design structure-based mutations in *Pyrococcus furiosus* Rad50 to alter protein core plasticity and residues undergoing ATP-driven movements within the catalytic domains. With this strategy we identify Rad50 separation-of-function mutants that either promote or destabilize the ATP-bound state. Crystal structures, X-ray scattering, biochemical assays, and functional analyses of mutant PfRad50 complexes show that the ATP-induced closed conformation promotes DNA end binding and end tethering, while hydrolysis-induced opening is essential for DNA resection. Reducing the stability of the ATP-bound state impairs DNA repair and Tel1 (ATM) checkpoint signaling in *Schizosaccharomyces pombe*, double-strand break resection in *Saccharomyces cerevisiae*, and ATM activation by human Mre11-Rad50-Nbs1 *in vitro*, supporting the generality of the *P. furiosus* Rad50 structure-based mutational analyses. These collective results suggest that ATP-dependent Rad50 conformations switch the Mre11-Rad50 complex between DNA tethering, ATM signaling, and 5′ strand resection, revealing molecular mechanisms regulating responses to DNA double-strand breaks.

Keywords DNA damage signaling; DNA repair; double-strand breaks; protein-DNA interactions

Subject Categories DNA Replication, Repair & Recombination; Structural Biology

DOI 10.1002/embj.201386100 | Received 26 June 2013 | Revised 25 November 2013 | Accepted 28 November 2013 | Published online 3 February 2014

EMBO Journal (2014) 33, 482–500

Introduction

Repair of DNA double-strand breaks (DSBs), arising from internal or external sources of damage and generally lethal if unrepaired, is achieved through non-homologous end joining (NHEJ) or homologous recombination (HR) (Krogh & Symington, 2004). The Mre11-Rad50-Nbs1(Xrs2)(MRN/X) complex plays central roles in both of these pathways and is conserved in all domains of life, as Mre11-Rad50 (MR) in prokaryotes and as MRN/X in eukaryotes (Lamarche *et al*, 2010; Stracker & Petrini, 2011). Mre11 forms a DNA-binding dimer that contains phosphoesterase motifs and is active as an exo- and endonuclease *in vitro* (Paull & Gellert, 1998; Williams *et al*, 2008), while Rad50 contains ATP-binding motifs and is similar in domain configuration to the structural maintenance of chromosomes ATPase family of proteins that regulate the activities and topology of chromosomal DNA (Williams *et al*, 2007). The eukaryote-specific Nbs1(Xrs2) protein contains phosphoprotein-binding FHA and BRCT motifs, regulates MR catalytic activities and flexibly links the complex to the checkpoint kinase ATM (Tel1) (Lee & Paull, 2007; Williams *et al*, 2009). Besides its DSB-related functions, MRN/X complexes also promote replisome stability in yeast and in mammalian cells (Doksani *et al*, 2009; Schlacher *et al*, 2011; Tittel-Elmer *et al*, 2009).

Rad50 ATP-regulated activities are essential for all MRN roles in DNA repair and signaling, as mutations in the Walker A or signature motifs exhibit phenotypes equivalent to a *rad50* deletion *in vivo* (Alani *et al*, 1990; Bhaskara *et al*, 2007; Chen *et al*, 2005; Moncalian *et al*, 2004). Recent MR structures illuminate the physical interactions between Mre11 and Rad50 in both the nucleotide-free and ATP-bound states, and reveal that Rad50 ATP binding results in extensive conformational changes at the base of the Rad50 coiled-coils (Lammens *et al*, 2011; Lim *et al*, 2011; Mockel *et al*,

1 The Department of Molecular Genetics and Microbiology, The Howard Hughes Medical Institute, Institute for Cellular and Molecular Biology, The University of Texas at Austin, Austin, TX, USA
2 Life Sciences Division, Lawrence Berkeley National Laboratory, Berkeley, CA, USA
3 The Scripps Research Institute, La Jolla, CA, USA
4 Department of Health and Human Services, Laboratory of Structural Biology, National Institute of Environmental Health Sciences, US National Institutes of Health, Research Triangle Park, NC, USA
5 Physical Biosciences Division, Lawrence Berkeley National Laboratory, Berkeley, CA, USA
6 The Skaggs Institute for Chemical Biology, La Jolla, CA, USA
*Corresponding author. Tel: 512 232 7802; Fax: 512 471 3730; E-mail: tpaull@mail.utexas.edu
**Corresponding author. Tel: 510 495 2404; Fax: 510 486 6880; E-mail: jat@scripps.edu
†These authors contributed equally to this work.

2011; Williams *et al*, 2011). Despite these informative structures and many years of research, however, the relationships between MR conformations and biological functions remain enigmatic. Specifically, we do not know: (i) what the function of the ATP-bound complex is, (ii) how ATP hydrolysis controls the functions of MR complexes on DNA, including the nuclease activity of Mre11, or (iii) why the rate of ATP hydrolysis is extremely slow.

To address these three unknowns and probe the relationships between MR conformations and functions, here we alter the stability of the ATP-bound state with engineered mutations and determine how the biological functions of MRN are affected, both *in vitro* and *in vivo*. Through structure-based mutations, four new Rad50 crystal structures, small-angle X-ray scattering (SAXS), biochemical assays, and *in vivo* DNA repair assays of these mutants, we find that Rad50 conformational switches regulate the stability of the ATP-bound dimer, and that this ATP-bound conformation promotes both DNA end binding and end tethering. In contrast, release from this ATP-bound state during hydrolysis is required for the endonuclease activity of Mre11 and the promotion of DNA end resection. Furthermore, we show the importance of wild-type (WT) levels of ATP binding and hydrolysis for DSB repair and signaling through ATM *in vivo*. These results reveal relationships between the ATP-driven conformational changes in Mre11 and Rad50 and the biological functions of the complex and suggest how ATP hydrolysis by Rad50 controls the balance between DNA end bridging and DNA resection.

Results

A Rad50 core cavity provides plasticity for ATP-driven conformational changes

Crystal structures of MR catalytic domains (MRcd) from bacteria and archaea suggest that the complex transitions from an ATP-free open conformation (PDB 3QG5) to an ATP-bound, compact conformation (PDB 3THO, 3AV0) with Rad50 altering access to the Mre11 nuclease active site (Lammens *et al*, 2011; Lim *et al*, 2011; Mockel *et al*, 2011; Williams *et al*, 2011) (Fig 1A). To determine if the conformation of MR seen in nucleotide-bound crystal structures resembles those in solution, we used SAXS, which can provide accurate models of conformations and assemblies in solution (Putnam *et al*, 2007; Rambo & Tainer, 2013a). Examining SAXS data from *P. furiosus* MRcd by Porod-Debye analysis shows the scattering intensity transitions from decaying with the 3rd power to the 4th power of the scattering angle when going from ATP-free to ATP-bound states, suggesting that upon ATP binding MRcd changes from a flexible assembly with many conformations to a single compact conformation (Rambo & Tainer, 2011). Furthermore, comparison of our experimental SAXS scattering of *P. furiosus* MRcd (Williams *et al*, 2011) to calculated SAXS profiles of *Methanococcus jannaschii* and *Thermotoga maritima* MR nucleotide bound states (Lim *et al*, 2011; Mockel *et al*, 2011) reveals that a single ATP-bound MR conformation exists in solution that matches the crystal structures based upon unbiased χ^2_{free} analysis (Fig 1B) (Rambo & Tainer, 2013a,b).

To examine the underlying mechanics of ATP-regulated conformational changes, we did a detailed analysis of Rad50 nucleotide-free and -bound structures. In the nucleotide-free state, a solvent-accessible channel extends deep into the Rad50 hydrophobic protein core (Fig 1C, Supplementary Movie 1). This conduit forms at the interface of the N- and C-terminal ABC-ATPase halves and is substantially remodeled with ATPase subdomain rotation in response to ATP binding. Concerted movement of R805 and R797 residues, which are implicated in Rad50 subdomain rotation and critical for DSB repair (Williams *et al*, 2011), block the conduit from the protein surface and partially fill the remaining cavity upon ATP binding (Fig 1D and Supplementary Movie 2). To accommodate these changes, conserved hydrophobic signature helix residues (L802 and L806) lining the channel rearrange with nucleotide binding. The L802 and L806 residues are displaced and L802 flips conformations, thereby reconstructing the protein core. In the ATP-bound state, a core cavity remains at the intersection between N- and C-terminal ATPase halves, but shrinks in size (from ~600 Å^3 to ~450 Å^3). Structural interpolations between unbound and ATP-bound states (Supplementary Movies 1 and 2) suggest that R805 sliding through the cavity facilitates precise domain realignment concomitant with the 35° subdomain rotation that occurs between the N- and C-terminal ATPase halves. Based on these observations, we hypothesized that the Rad50 core cavity imparts structural plasticity to facilitate ATP-regulated conformational changes.

If the Rad50 core cavity identified here is functionally important, then a mutation designed to partially fill the cavity should impair ATP-dependent subdomain rotation and thus ATP binding. We therefore substituted more bulky hydrophobic Phe or Trp residues for the L802 and L806 residues that line the Rad50 cavity, and expressed these mutants in the Rad50cd-linked form, which connects the Rad50 N- and C-terminal domains with a short flexible linker (Supplementary Fig S1). We measured dimerization by incubating the proteins at a temperature appropriate for the *P. furiosus* thermophile (65°C for 10 min.), followed by gel filtration at room temperature. We found that the WT protein and the L806F variants formed ATP-dependent dimers in this assay, but the L802W variant failed to exhibit dimerization (Fig 2A and Supplementary Fig S1). We also analyzed nucleotide-induced changes in MRcd (Mre11 bound to the Rad50 catalytic domains, Rad50cd, which have a short region of coiled-coil in two separate polypeptides; Supplementary Fig S1). Using SAXS under trapping conditions (short period of high temperature incubation followed by flash cooling), we found L802W MRcd behaves the same as WT protein with and without ATP (Supplementary Fig S2). Yet, when SAXS data was collected with ATP and the temperature held at 65°C, the L802W mutant initially forms a closed/single compact structure, but returned to the open state by the end of the 8 min experiment, whereas the WT protein retained the compact conformation during this time course (Fig 2B and C). Thus the L802W mutation appears to destabilize the ATP-bound state as shown by the SAXS data and structural comparison map that provides a quantitative and superposition-independent evaluation of solution-state conformational differences (Hura *et al*, 2013). The destabilization appears to be linked to ATP hydrolysis, as the L802W MRcd compact form was stable over the same time course with ATPγS (Fig 2D).

To investigate the structural impact of the L802W mutation, we solved the X-ray crystal structure to 2.3 Å resolution in the absence of ATP (Table 1). As predicted, the bulky Trp residue extends into the space neighboring residue 802, and partially

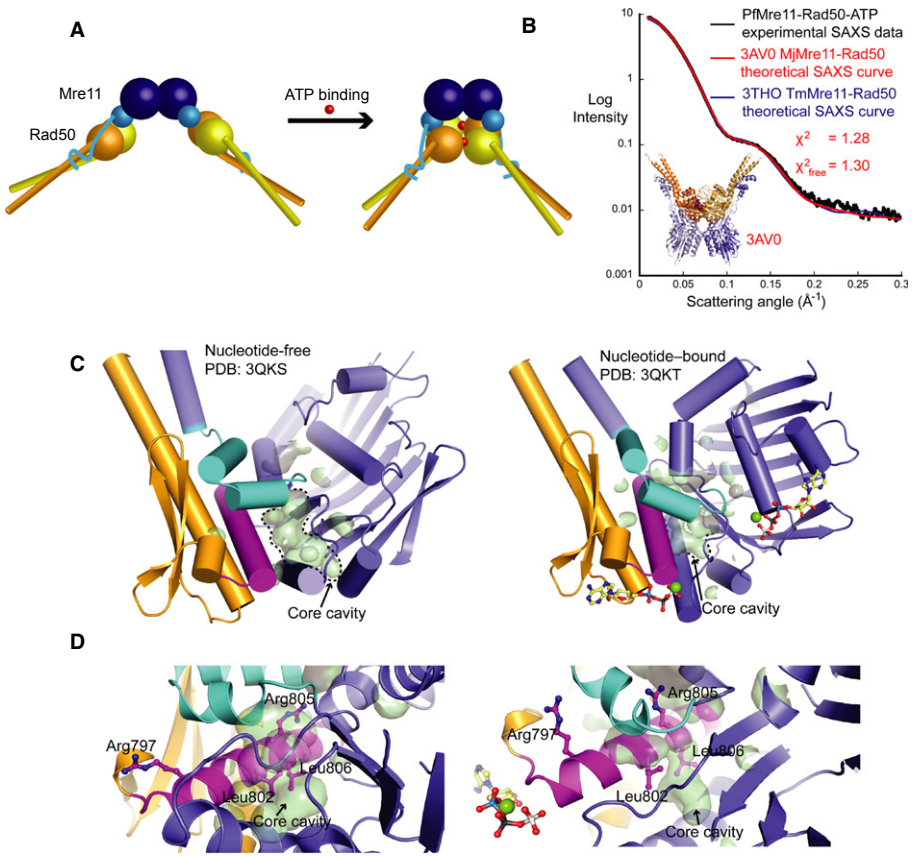

Figure 1. ATP induces conformational changes in Mre11 and Rad50.

A Schematic of Mre11 (blue) and Rad50 (orange, yellow) catalytic domains and conformational changes upon ATP binding.

B MR solution structure. Experimental SAXS data of ATP-bound *P. furiosus* Mre11-Rad50cd-linked in solution closely matches calculated SAXS scattering curves of MRcd crystal structures in nucleotide-bound states (example shown inset).

C Rad50 colored as follows: N-terminal lobe, blue; signature coupling helices, cyan; C-terminal lobe, orange; extended signature motif, magenta; core cavity, green surface. The cavity is remodeled as Rad50 rotates 35° between nucleotide states. See also Supplementary Movie 1.

D Close-up of Rad50 core cavity, basic-switch and core Leu residue changes between nucleotide-free (left) and nucleotide-bound (right) states. Colored as in (C), also see Supplementary Movie 2.

fills the protein core cavity (Fig 2E). To accommodate this mutation, the Rad50 core is partially remodeled and W802 blocks the space that R805 rotates upon ATP binding in WT Rad50. Although the overall ATPase fold is maintained, the L802W substitution distorts the relative positioning of the Rad50 N- and C-terminal ATPase subdomains. Rad50 ATP binding normally induces approximately 35° counterclockwise rotation of the N-terminal Rad50 ATPase subdomain relative to the C-terminal lobe. Intriguingly, the L802W cavity-filling mutant imparts a clockwise (~5° and ~9° with 9° shown in Fig 2F) ATPase sub domain over-rotation relative to WT Rad50, opposite to the direction induced by ATP binding. Thus, engineered hydrophobic core variants alter alignment of the mobile ATPase sub domains.

ATP-dependent Rad50 conformational changes in solution

To determine the effects of the cavity mutations on Rad50 conformation in solution, we established limited proteolysis assays. In these experiments, the proteins were first incubated at high temperature (65°C) for 10 min. prior to the trypsin cleavage reaction at 37°C. Tryptic digest of Rad50cd with ATP or ATPγS yields two unique approximately 17-kDa and 19-kDa bands (Fig 3A). We found that the ATP-dependent trypsin cleavage site maps to K155 on the second of two signature coupling helices (Williams *et al*, 2011) connecting the ATPase N-terminal lobe to the coiled-coil (Supplementary Table S1, Supplementary Fig S3), as confirmed by partial proteolysis of a Rad50cd-K155A mutant (Fig 3A). The K155 location suggests that ATP induces rotation between the N- and C-terminal Rad50 lobes and repositions the coiled-coil domains, increasing K155 flexibility and exposure to solution (Fig 3F). Similar trypsin cleavage sites are observed using Rad50cd that has been covalently linked by a short, flexible linker (Rad50cd-linked, Supplementary Fig S1).

Analysis of the L802W Rad50cd-linked protein by partial proteolysis showed that the mutant does not undergo K155 cleavage in the presence of ATP (Fig 3B). However, further analysis of L802W showed that the ATP-bound conformation is seen by proteolysis, but only with non-hydrolysable ATP analog ATPγS (Fig 3C). Thus,

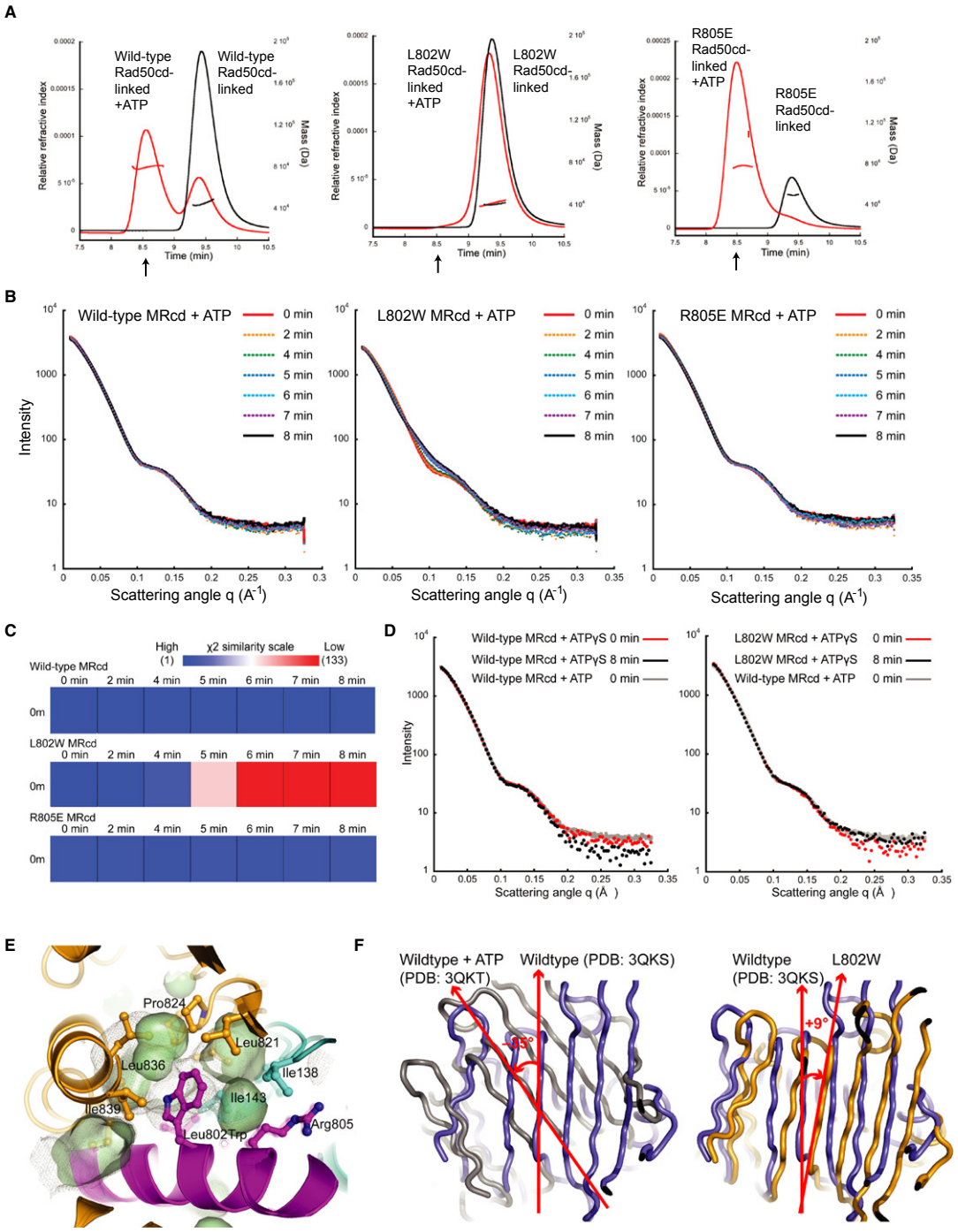

Figure 2. Rad50 cavity alterations destabilize the ATP-bound state.

A Gel filtration of Rad50cd-linked proteins with or without ATP. Lines across peaks represent molecular weights measured by MALS (right axis); arrows show positions of dimer peaks. See also Supplementary Fig S1.

B SAXS time-course assays showing scattering curves of MRcd WT, L802W, or R805E variants with 0.5 mM ATP at 65°C, plotted at the indicated time points.

C SAXS similarity matrices were made by comparing MRcd variant scattering curves for each time point in the SAXS time-course experiment, measured with ATP at 65°C, compared to the 0 min curve. As indicated by the scale, blue represents very high and red represents very low similarity of curves based on χ^2 scores.

D SAXS analysis of WT and L802W MRcd complexes in the presence of 0.5 mM ATP or ATPγS at 65°C as indicated.

E The L802W Rad50cd-linked structure, colored as in Fig 1C, is superimposed on WT Rad50cd-linked, with transparent coloring and cavity (dotted surface). The Trp substitution overlaps with the WT surface, remodeling the Rad50 core.

F ATP-driven conformational states. Superimposition of nucleotide-free Rad50 (blue) with nucleotide-bound Rad50 (gray, left) and nucleotide-free L802W Rad50 (orange, right) using C-terminal domain residues 741–785 for the alignment. N-terminal lobes are shown for clarity.

Table 1. X-ray diffraction data collection and refinement statistics

	P. furiosus Rad50 L802W (PDB 4NCH)	*P. furiosus* Rad50 R805E (PDB 4NCI)	*P. furiosus* Rad50 R805E + ADP/BeF (PDB 4NCJ)	*P. furiosus* Rad50 R797G (PDB 4NCK)
Data collection				
Space group	$P3_221$	$P2_12_12_1$	$P2_12_12_1$	$P22_12_1$
Cell dimensions				
a, b, c (Å)	70.4, 70.4, 282.0	68.0, 69.1, 74.5	83.0, 108.5, 148.7	49.7, 68.1, 203.0
α, β, γ (°)	90, 90, 120	90, 90, 90	90, 90, 90	90, 90, 90
Resolution (high res. bin) (Å)	46.1–2.30 (2.44–2.30)	37.2–2.30 (2.44–2.30)	45.4–2.00 (2.09–2.00)	48.2–2.00 (2.12–2.00)
I/σI (high res. bin)	14.2 (2.00)	16.6 (1.96)	16.0 (2.2)	16.4 (1.61)
R_{meas} (%)	5.5 (73.2)	4.7 (86.7)	7.9 (70.1)	4.0 (69.5)
CC (1/2)	99.8 (63.9)	99.9 (67.6)	99.8 (78.1)	99.9 (70.6)
Completeness (%)	99.5 (99.2)	99.9 (99.8)	98.0 (100)	99.0 (99.9)
Total observations	203637	116839	705952	298108
Unique observations	37288	16102	90187	47574
Redundancy	5.5	7.3	7.9	6.3
Wilson B-factor	52	56	28	43
Collected at beamlines	SSRL11-1	SSRL11-1	ALS 8.3.1	ALS 8.3.1
	ALS 12.3.1	ALS 12.3.1	ALS 12.3.1	ALS 12.3.1
Refinement				
Resolution (Å)	46.1–2.30	37.2–2.30	45.4–2.00	48.2–2.0
R_{work}/R_{free}	0.2069/0.2462	0.2015/0.2583	0.2309/0.2618	0.1868/0.2311
Mole per ASU	2	1	8	2
No. of atoms	9446	4949	21267	9577
Macromolecule	4592	2398	10012	4662
Ligand/ions	15	–	128	7
Waters	329	172	846	324
B-factors	57.8	69.9	39	58
Macromolecule	58.3	70.2	39	58.1
Ligand/ions	43.3	–	21.9	106.3
Waters	51.3	65.3	42.7	55
r.m.s. deviations				
Bond lengths (A)	0.003	0.003	0.008	0.008
Bond angles (°)	0.68	0.73	1.17	1.07
Ramachandran favored (%)	96	93	97	96
Ramachandran outliers (%)	0.33	0.32	0.87	1.3
Clashscore	3.08	3.58	7.84	5.76

the L802W mutation does not block ATP binding, but instead destabilizes the ATP-dimerized state, consistent with the SAXS results showing instability of the ATP-bound compact structure of MRcd L802W in solution at high temperature (Fig 2).

To examine the effect of Mre11 and the Rad50 coiled-coil, the solution conformation of Rad50 was also tested using complexes of MRcd (Supplementary Fig S3) and the full-length MR complex (Fig 3D). Results with both of these complexes showed that the K63 residue in Rad50 is cleaved by trypsin in the absence of ATP but is approximately 100% protected by nucleotide (Fig 3F and Supplementary Table S1), indicating solution structures resemble crystal structures that show that K63 is relatively inaccessible in the ATP-bound state but exposed in the unbound state. Reduced protection of the K63 cleavage site in catalytic mutants (S793R and K36A) confirms the nucleotide specificity of the proteolysis protection (Fig 3D). In this assay, the L802W mutation reduced the ATP-dependent protection of the K63 cleavage site in Rad50 (Fig 3E). Thus proteolysis results with the Rad50 catalytic domains, MRcd, and full-length MR all show that the L802W mutation destabilizes the ATP-bound state. The K155 trypsin cleavage site is not observed in full-length MR as it is protected by Mre11 binding (see Supplementary Fig S3). Notably, Mre11 cleavage by trypsin is also altered

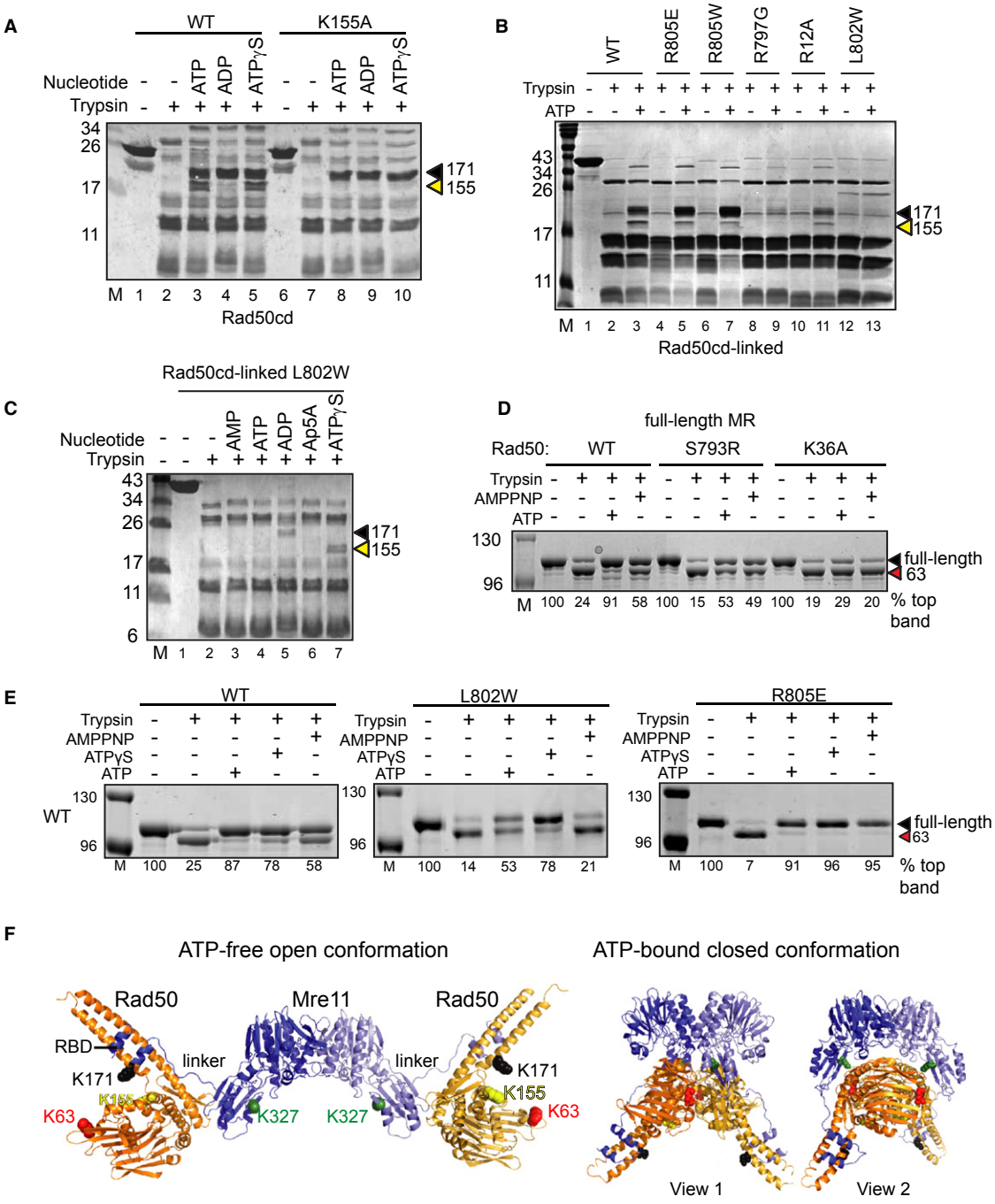

Figure 3. ATP binding promotes conformational changes in Rad50 that are measurable by partial proteolysis.

A Rad50cd (5 μg) proteolysis with indicated nucleotides revealing distinct conformational states. Triangles show ATP-stimulated products of proteolysis at K155 (yellow triangle) and K171 (black triangle).

B Proteolysis of Rad50cd-linked (5 μg) variants with ATP as in (A).

C Proteolysis of Rad50cd-linked L802W (5 μg) with indicated nucleotides as in (A).

D, E Proteolysis of full-length WT or mutant MR (1 μg Rad50) with nucleotide. Red triangle indicates K63 cleavage product. Quantitated levels of undigested protein are shown below each lane. Also see Supplementary Fig S3 and Supplementary Table S1.

F Structural models of the ATP-free and ATP-bound MRcd generated from Mre11-Rad50 structures from PDB ID 3QKS (open) and PDB ID 3QKU (closed) superimposed with *T. maritima* MR (PDB ID 3QG5; open) and *M. jannaschii* MR (PDB ID 3AV0; closed). Locations of tryptic digest sites are mapped, with two views of the closed model shown for clarity. Residues 327 to 357 of Mre11 are in the linker region; residues 394–404 are outside of the region that was crystallized.

Source data are available online for this figure.

by ATP (Supplementary Fig S3), indicating changes in Mre11 structure with Rad50 nucleotide binding that experimentally support structural predictions (Lammens *et al*, 2011; Lim *et al*, 2011; Mockel *et al*, 2011; Williams *et al*, 2011).

Rad50 Arg-switch mutations increase ATP-bound dimer stability

Based on Rad50 crystal structures, arginine residues 797 and 805 were hypothesized to be switches for transitions between the open and closed MR states (Williams *et al*, 2011). To test this, R797G and R805E mutations were made in Rad50cd-linked, MRcd, and full-length MR complexes and analyzed as described above. Similar to L802W, R797G Rad50cd-linked protein also showed decreased dimerization with ATP (Supplementary Fig S1); however, the R805E mutant showed more efficient dimerization than WT Rad50 (Fig 2A). Partial proteolysis of R805E did not show significant differences from WT Rad50 complexes except that R805E confers higher protection from trypsin cleavage at K63 in the presence of ATP and non-hydrolyzable nucleotides in MRcd and in full-length MR, and also is dominant over the destabilizing effects of the L802W mutation (Fig 3E, Supplementary Fig S3).

Rad50 R805E and L802W mutations alter ATP binding and hydrolysis

To test the effect of Rad50 cavity and Arg-switch mutations in more detail, we focused on the R805E and L802W variants with the greatest impact on ATP-induced dimerization of Rad50. To assess ATP binding directly, we used full-length MR and measured binding of a fluorescent ATP derivative, 2′,3′-O-(2,4,6-Trinitrophenyl) ATP (TNP-ATP), as was done for other enzymes (Hiratsuka, 1976). With MR, we found that increasing concentrations of TNP-ATP quenched the intrinsic fluorescence of tryptophan residues in Rad50 (likely W782 based on proximity to the bound nucleotide (Hopfner *et al*, 2000)) as shown in Fig 4A and B. Both the L802W and R805E full-length complexes showed equivalent binding to TNP-ATP, thus the differences observed in ATP-induced conformational changes are not due to loss of nucleotide binding capacity. We also confirmed that TNP-ATP exhibited similar effects on the WT and mutant proteins in the partial proteolysis assay compared to ATP (Supplementary Fig S4) and that TNP-ATP competes with ATP in hydrolysis assays with full-length MR (Supplementary Fig S4).

Analysis of the ATPase activities of the WT and mutant proteins shows differences in hydrolysis kinetics and also in stimulatory effects of Mre11 and the coiled-coils on Rad50 catalytic activity (Fig 4C, Supplementary Fig S4). The full-length MR complex exhibits lower affinity for ATP but a 100-fold higher k_{cat} for ATP hydrolysis compared to the Rad50 catalytic domain alone, likely due to physical attachments between the domains that are mediated by both Mre11 and the Rad50 coiled-coils. The R805E protein shows an increase in ATP affinity compared to the WT enzyme (3-fold in the Rad50cd-linked form and ~100-fold in the full-length protein), consistent with the higher efficiency of ATP-induced conformational changes seen with this mutant. The L802W mutant, in contrast, primarily exhibits an increase in k_{cat} relative to the WT protein, which is most dramatic in the Rad50cd-linked form. In the full-length MR complex, the kinetic parameters of the L802W complex are more similar to WT, reflecting the strong effects of the coiled-coil and Mre11 attachments on ATPase activity.

ATP-dependent changes in Rad50 conformation control DNA binding

To measure DNA binding by Rad50cd-linked, MRcd, and full-length MR, we used gel mobility shift assays with double-stranded DNA substrates (Fig 4D–F). All of the WT proteins formed a large ATP-dependent complex (I) plus a smaller ATP-independent complex (II) and exhibited ATP-stimulated DNA binding, extending prior measurements with Rad50 ATPase domains only (Hopfner *et al*, 2000). In contrast, L802W Rad50cd-linked and MRcd complexes did not bind DNA in the presence of ATP but did form a complex with ATPγS (Fig 4D, E). These Rad50cd-linked results agree with the K155 partial proteolysis pattern, suggesting that reorganization of the catalytic domains into the ATP-driven closed conformation drives formation of the large protein-DNA structures observed in the gel shift assay. To examine the contribution of the coiled-coils to DNA binding, full-length proteins were also tested in gel shift assays, which showed that L802W MR does exhibit ATP-dependent binding like the WT protein, yet the mobility of complexes is reduced (Fig. 4F). The Rad50 coiled-coils thus have a stabilizing effect on Mre11-Rad50 DNA binding. In contrast to L802W, the R805E Rad50cd-linked and MRcd complexes bound DNA similarly to WT with ATP, and even more efficiently with ATPγS. Surprisingly, both R805E and R797G full-length MR exhibited ATP-independent as well as ATP-dependent DNA binding, which is not observed with the WT enzyme.

To examine the structural basis for the differential abilities of the Rad50 cavity and Arg-switch variants to form the ATP-bound state, we solved structures of Rad50 R797G and R805E without nucleotide and R805E with an ATP mimic, ADP-BeF-Mg^{2+} (Table 1). These structures show that the mutations remove R797 and R805, which act in salt-bridge interactions, without distorting the local fold. In contrast to the over-rotated state found for L802W, the R805E and R797G structures show small but significant alteration of overall subdomain orientation compared to WT: notably both were rotated/translated (~3°) towards the ATP-bound state.

Interestingly, R797G and L802W share a common feature: increased flexibility in the D-loop region (residues 827–833) that immediately follows the Walker B box. In WT Rad50, this loop is flexible in the absence of ATP and becomes ordered as it packs with H855 (of the His-loop) in the neighboring Rad50 subunit of the dimer. In comparison to WT, residues on this loop in the R797G structure have less-well defined electron density and higher temperature-factors, and in the L802W structure these residues are disordered (Supplementary Fig S4). While crystal packing may stabilize the D-loop in the WT structure, increased flexibility of a loop that becomes ordered in the ATP-bound dimer interface should destabilize but not block the formation of the ATP-bound state.

The overall structure of Rad50 R805E bound to ADP-BeF-Mg^{2+} resembles the WT protein bound to nucleotide. However, a key difference is seen in the active site with E823, the Walker B glutamic acid that charges the attacking water and is essential for ATP hydrolysis, displaced by 2 Å with an additional water molecule filling the void (Supplementary Fig S4). Similarity

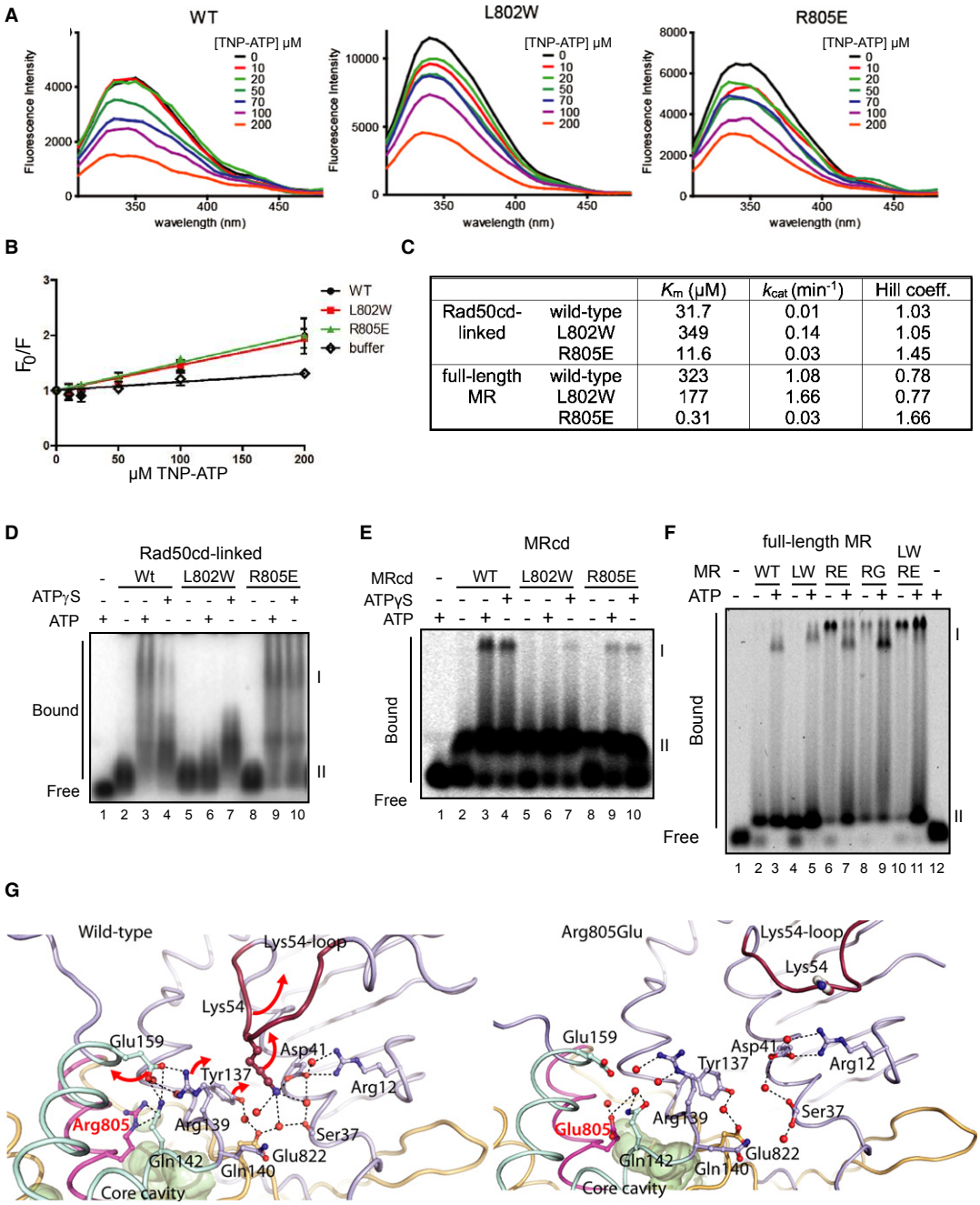

		K_m (μM)	k_{cat} (min^{-1})	Hill coeff.
Rad50cd-linked	wild-type	31.7	0.01	1.03
	L802W	349	0.14	1.05
	R805E	11.6	0.03	1.45
full-length MR	wild-type	323	1.08	0.78
	L802W	177	1.66	0.77
	R805E	0.31	0.03	1.66

Figure 4. Rad50 catalytic domain mutations affect ATP-dependent DNA binding and hydrolysis.

A ATP binding by full-length MR complexes as measured by quenching of tryptophan fluorescence by TNP-ATP. Shown are emission scans using 290 nm excitation and TNP-ATP as indicated.

B Quantitation of quenching efficiency (F_0/F) at 330 nm emission calculated from (A).

C ATPase kinetics measurements of Rad50cd-linked and full-length MR proteins (see also Supplementary Fig S4).

D Gel-shift assays of Rad50cd-linked (2.5 μM) with a 41-bp DNA duplex substrate.

E Gel-shift assays of MRcd complexes (400 nM) with a 41-bp DNA duplex substrate. Protein-DNA complexes are indicated (I and II), with the upper band (I) being nucleotide-dependent.

F Gel-shift assays as in (E) with full-length MR (200 nM).

G Crystal structures reveal hydrogen-bonding rearrangements between nucleotide-free WT (left) and R805E Rad50cd-linked (right). Colored as in Fig 1C, with the K54 loop in burgundy and red arrows highlighting major changes. See also Supplementary Fig S4.

Source data are available online for this figure.

between the coordination of active site residues in the R805E mutant and those in the transition state of MalK (Oldham *et al*, 2007), a related ABC-ATPase, suggests that this alignment contributes to more efficient ATP binding and mimics a previously unseen Rad50 functional intermediate.

Unique features of the R805E structure without ATP suggest how this mutant binds to ATP more strongly than WT. The R805E mutation disrupts a hydrogen-bonding network of R805, E159, R139, Y137 and Q142, with a net separation of these residues. This conformational rearrangement alters a neighboring hydrogen bonding network of Y157, R12, D41, D60 and K54, a residue linked to DNA binding. In the ATP-free state these disruptions displace the loop containing K54 and D60, toward a solvent-accessible position (Fig 4G). This shift partially mimics the conformational change that occurs in WT Rad50 upon ATP binding, where the switch of R12 to bind nucleotide releases K54 to the protein surface. This Rad50 monomer destabilization may explain the increased stability of the ATP-induced dimer and, in full-length MR, the displacement of the K54 loop may be sufficient to form a DNA binding surface between Rad50 monomers in the complex. Interestingly, deletion of the entire loop containing K54 (Δ51–60) eliminates the ATP-stimulated DNA binding of full-length MR (Supplementary Fig S4), suggesting that this loop conformation is important for ATP-induced DNA contacts.

DNA end tethering by MR is an ATP-dependent function of Rad50

To test ATP impact on DNA repair functions including DSB end bridging, we established an end-tethering assay: preincubation of Mre11-Rad50 with linear DNA containing cohesive ends, followed by incubation with a DNA ligase. We found that the presence of full-length MR during preincubation promoted DNA ligation into multimeric products in an ATP-dependent manner (Fig 5A). Using full-length Mre11 and Rad50 separately, we found that DNA end tethering was largely a function of Rad50 (Fig 5B, lanes 8 and 10). Rad50 alone supports end tethering at a similar concentration to full-length MR, yet bridging by Mre11 alone required >10-fold higher concentrations (lane 12). Rad50 DNA end tethering requires additional domains not present in the catalytic head domains since Rad50cd-linked, which lacks the Zn-hook and most of the coiled-coil domains, required 100-fold higher concentrations compared to full-length Rad50 (Fig 5B,C). The presence of Mre11 also improved DNA end tethering by the Rad50 catalytic head domains, as seen with the MRcd complex that supported end ligation at 4-fold higher concentrations than full-length MR (Fig 5D). DNA end tethering did not require Mre11 nuclease activity as the nuclease deficient Mre11-H85L mutant complex supported ligation (Fig 5E). Our results show that a physical connection between the two Rad50 catalytic domains, either through the coiled-coils and Zn-hook or through Mre11, is important for DNA end tethering by MR. The preference for ATP over AMP-PNP may reflect reduced ability of AMP-PNP to form the closed complex (see Fig 3E) rather than a requirement for ATP hydrolysis.

The ATP-bound Rad50 conformation promotes DNA end binding

Analysis of the end tethering ability of the mutants in either MRcd (Fig 5F) or full-length MR (Fig 5G) showed that L802W Rad50 exhibits similar activity to WT, while R805E and R797G Rad50 variants show higher levels of tethering and strikingly even promote tethering without ATP (Fig 5G). Thus, efficient end tethering/bridging is correlated with stable ATP binding and DNA binding.

MR has a general affinity for DNA. To examine specificity for DNA ends, a circular competitor DNA was included with the idea that longer occupancy on DNA ends may result in better specificity for ends over unbroken DNA (Fig 5H). When the substrate was added before the competitor, WT full-length MR end-bridging was mostly blocked by the competitor DNA (lane 6), whereas tethering was completely blocked when the competitor was added before the substrate (lanes 7, 8). While the L802W mutant behaved similarly to WT, the R805E mutant tethered ends efficiently with competitor, even when competitor DNA was added first (Fig 5H, lanes 15, 16). Thus the R805E mutants are more efficient than WT MR in this assay and show a preference for DNA with ends, suggesting that the ATP-bound conformation binds with high specificity to DNA ends. Importantly, this ligation-mediated tethering assay supports and extends scanning force microscopy studies of MR complexes bridging multiple DNA molecules (de Jager *et al*, 2001); it is nucleotide-dependent, and is altered by single amino acid changes in the Rad50 catalytic domain.

The ATP-bound conformation of Rad50 is insufficient for DNA end resection

To test the endonuclease activities of WT and mutant full-length MR, the complexes were incubated with a 700 bp DNA substrate containing a fluorescent Cy3 label on one 5′ end (Fig 6A). WT MR removes 5′ oligonucleotides from this substrate in an ATP-dependent manner in $MgCl_2$ (Hopkins & Paull, 2008). All mutant complexes showed activity in this assay. Yet, the L802W mutant was more efficient at 5′ strand cleavage compared to WT whereas R805E was reduced in nuclease activity. Little activity is seen on the 3′ strand of linear DNA with WT MR, but the labeled 3′ end was removed efficiently by the L802W complex (Fig 6B). Interestingly, the coiled-coil and Zn-hook domains are important for Mre11 endonuclease activity as the WT MRcd complex fails to exhibit significant nuclease activity in comparison to the full-length complex (Fig 6C). The nuclease differences between MR mutants are not as striking when the complexes are assayed for 3′–5′ exonuclease activity in the presence of manganese (Fig 6D).

DSB repair by homologous recombination requires extensive 5′ end resection to create 3′ single-stranded tails, and MR stimulates the helicase-nuclease complex HerA-NurA to carry out long-range resection of DNA *in vitro* (Hopkins & Paull, 2008). To test the effect of the L802W and R805E mutations on this recruitment, we assayed our mutants in a DNA resection assay in combination with the HerA-NurA complex (Fig 6E). WT full-length MR increased the degradation of the plasmid substrate by HerA-NurA 7- to 8-fold, as did the L802W mutant (Fig 6E, lanes 4–6 and 8–10). In contrast, the R805E mutant failed to promote HerA-NurA activity (lanes 12–14). Thus stable ATP binding (i.e. slow hydrolysis) is correlated with stable DNA binding and stable DNA tethering, but low levels of DNA end cleavage, as seen with the R805E mutant. In contrast, unstable ATP binding is associated with unstable DNA binding, low efficiency DNA tethering and high levels of DNA end cleavage as seen with the L802W mutant.

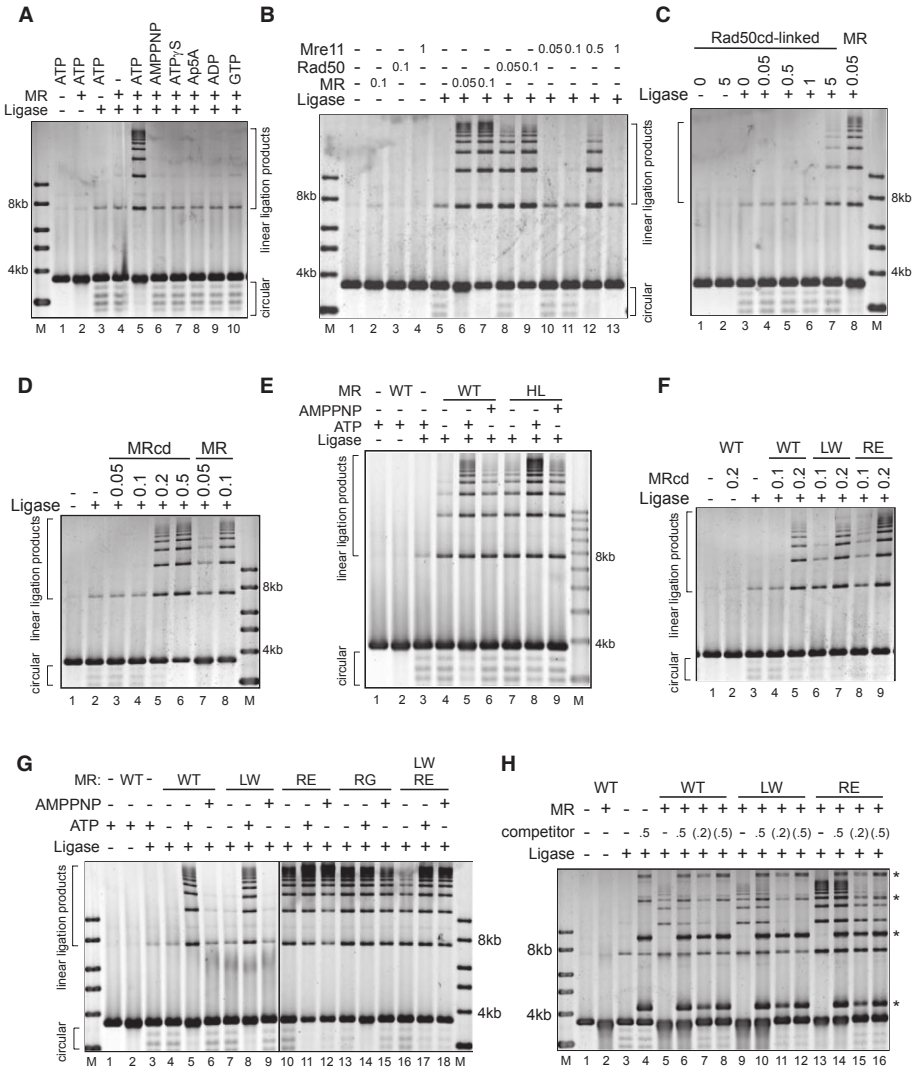

Figure 5. DNA end tethering by MR and designed mutants.

A Full-length MR (50 nM) was assayed for DNA end tethering with pCDF-1b plasmid, nucleotide, and *E. coli* DNA ligase (NAD-dependent) as indicated.

B Assays were performed as in (A) with Rad50 (50 nM or as indicated) and Mre11.

C Assays were performed as in (A) with Rad50cd-linked.

D Assays were performed as in (A) with MRcd.

E Assays were performed as in (A) with full-length wt MR and nuclease-deficient MR (Mre11 H85L).

F Assays were performed as in (A) with MRcd Rad50 variants as indicated.

G Assays were performed as in (A) with full-length MR Rad50 variants.

H DNA end tethering assays were performed as in (A) with the indicated addition of supercoiled pCDF-1b competitor DNA.

Data information: Reactions in lanes 4, 6, 10, and 14: substrate added before competitor; reactions in lanes 7, 8, 11, 12, 15, and 16: competitor added before substrate (* indicates positions of competitor DNA). Numbers indicate relative amount of competitor vs. substrate DNA. Ligation products (circular and multimer-linear) are indicated.

Source data are available online for this figure.

DNA resection requires Rad50 head domain opening following ATP hydrolysis

If DNA end tethering and resection activities oppose each other and are regulated by the conformational changes that accompany ATP binding and hydrolysis, it should be possible to regulate these activities by regulating Rad50 catalytic domain dimerization. To test this hypothesis, we introduced cysteines into the Rad50 ATPase domains at positions that would be in close contact only in the ATP-bound state (D55C and T790C, Fig 7A) based on the AMP-PNP-bound Rad50 crystal structure (Hopfner *et al*, 2000). Using this system, dimerization can be monitored

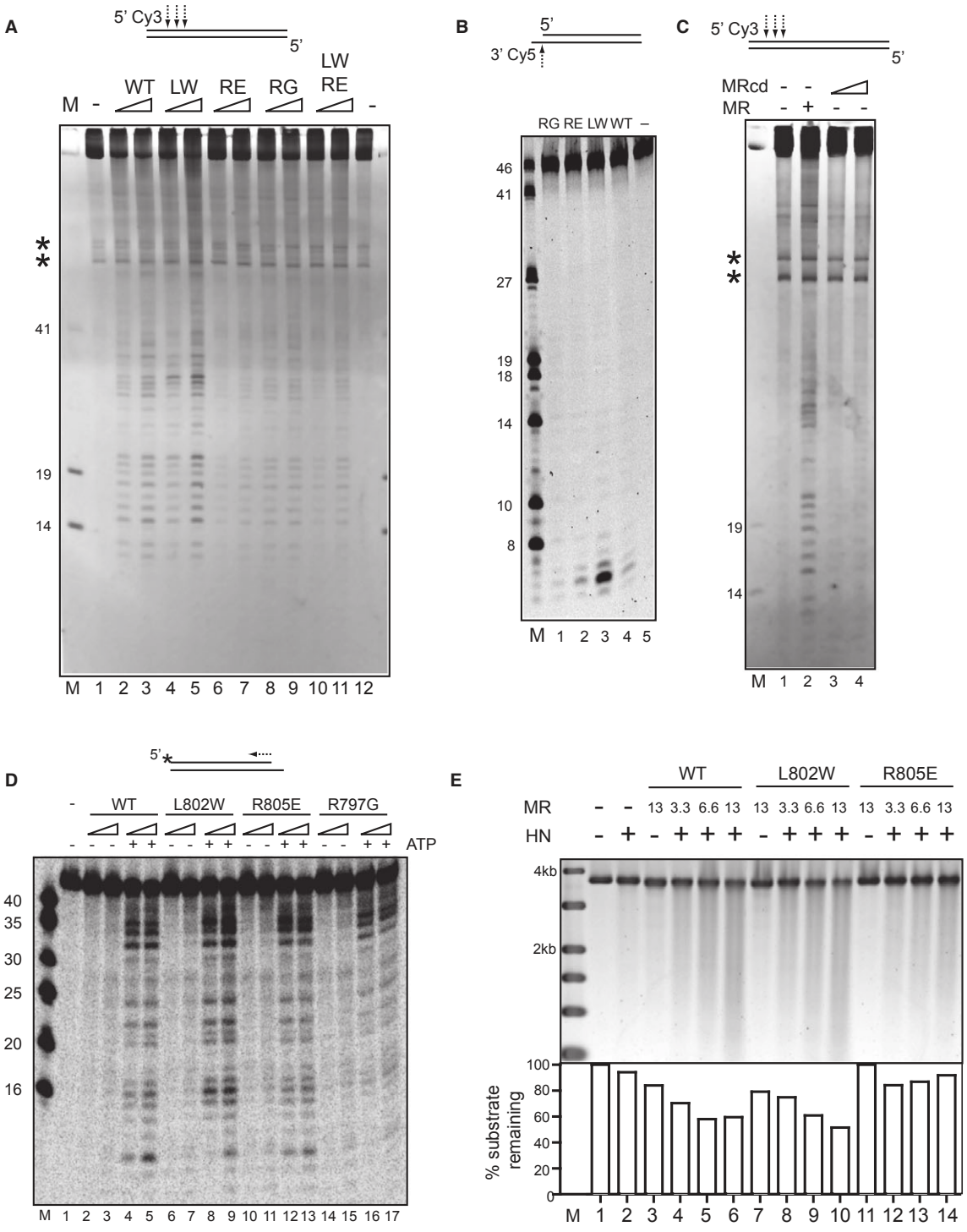

Figure 6. Rad50 separation-of-function mutations affect MR nuclease activity.

A Endonuclease assay for full-length MR variants (300 and 600 nM) on a 717-bp double-stranded DNA substrate. The shorter oligonucleotides are endonucleolytic products, except bands marked with *.

B Nuclease assay as in (A), but with a 41-bp double-stranded DNA substrate.

C Nuclease assay as in (A), with WT full-length MR (0.9 μM) and MRcd (1 and 2.5 μM).

D Exonuclease assay for full-length MR variants (100 and 200 nM) using a 41-bp double-stranded DNA, labeled on the 5′ end of the top strand with $_{32}$P (*).

E Resection assays with full-length MR (nM concentrations as indicated), HerA and NurA (HN) with a 3.8-kb linearized plasmid.

Source data are available online for this figure.

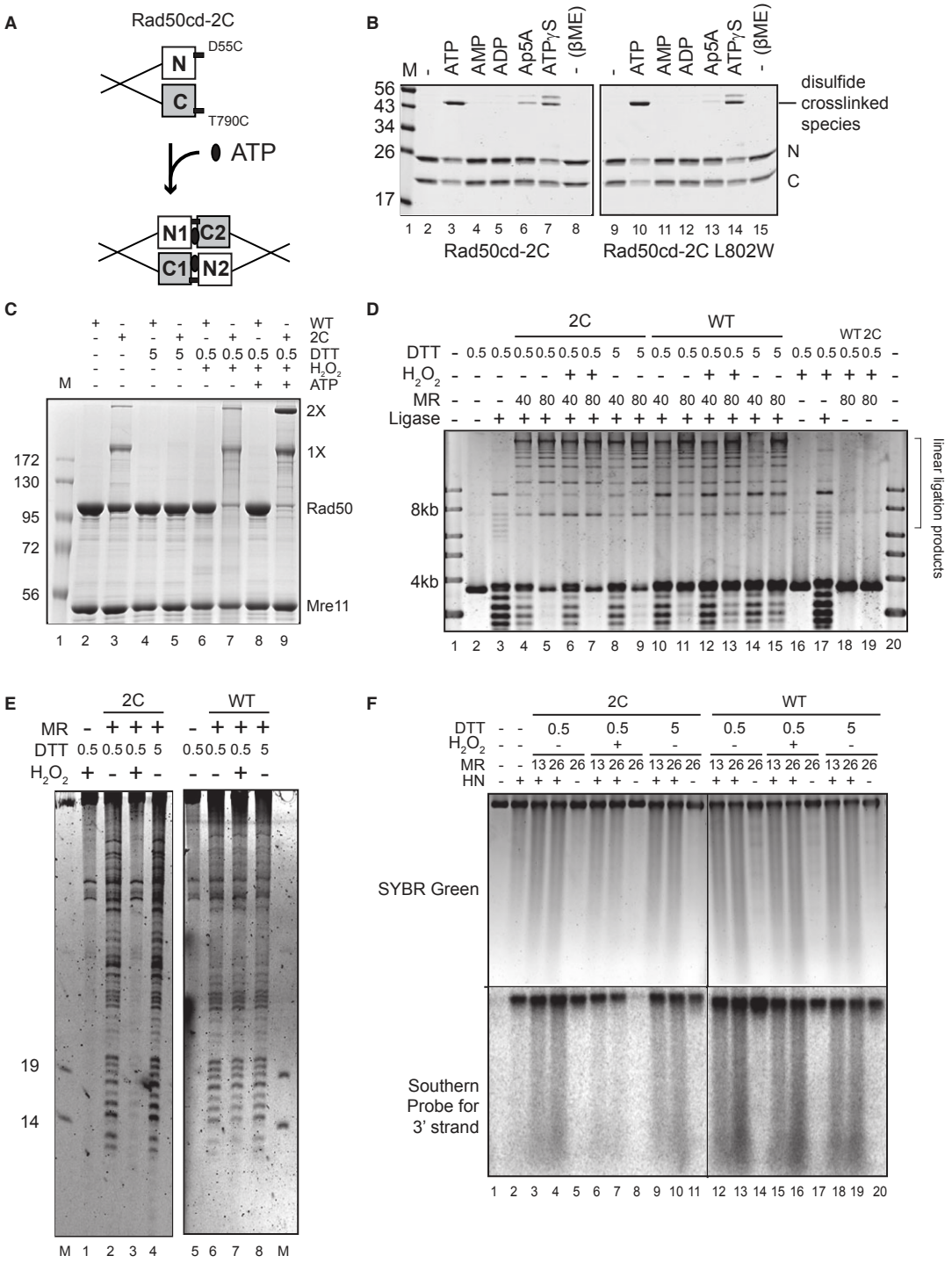

Figure 7. Cross-linking of Rad50 ATPase domains blocks DNA end resection.

A Crosslinking scheme uses introduced cysteines that are brought close enough to form disulfide bonds when Rad50 dimerizes with ATP.

B Crosslinking of Rad50cd-2C variants (3.5 μM) with indicated nucleotides (0.5 mM ATP or 2 mM other nucleotides), separated by SDS–PAGE in the absence of reducing agent except in lanes marked βME.

C Full-length MR or MR-2C proteins (2.35 μM) were cross-linked with H_2O_2 (2 mM) with DTT (mM) and ATP (0.5 mM) as indicated.

D Cross-linked full-length MR and MR-2C (nM) were assayed for DNA end tethering as in Fig 5A with H_2O_2 (2 mM), DTT (mM) and T4 DNA ligase added as shown.

E MR-2C (1.6 μM) and full-length MR (0.9 μM) were tested for endonuclease activity as in Fig 6A following crosslinking with DTT (mM) and H_2O_2 (2 mM) as indicated.

F MR-2C and full-length MR (nM) were cross-linked with DTT (mM) and H_2O_2 (2 mM) as indicated and assayed for plasmid resection as in Fig 6D. Also see Supplementary Fig S5.

Source data are available online for this figure.

by disulfide-crosslinking of Rad50 ATPase domains on SDS-PAGE gels in the absence of reducing agents. When the cysteine mutations were made in Rad50cd (Rad50cd-2C), efficient crosslinking was dependent on ATP (or ATPγS) (Fig 7B), and dimers accumulated during the reaction since the ATPase domains cannot release following ATP hydrolysis. In these assays, the L802W mutant also formed the crosslinked species similar to WT Rad50 with ATP or ATPγS. The dinucleotide Ap5A showed a weak effect in stimulating crosslinking of the Rad50cd complexes (Fig 7B) but did not mimic ATP in the partial proteolysis or ligation assays (Figs 3C and 5A), thus the adenylate kinase activity of Rad50 (Bhaskara *et al*, 2007) does not appear to play a major role in promoting the conformational changes in Rad50 characterized here.

In full-length MR (MR-2C), disulfide crosslinks were formed in an ATP-stimulated manner and were promoted by H_2O_2 oxidation, although in this case there was also a basal level of ATP-independent crosslink formation (Fig 7C, lanes 7, 9), consistent with SAXS data showing flexible MRcd that likely samples a closed state before becoming fully closed upon ATP binding (Williams *et al*, 2011). WT MR did not form crosslinks despite having naturally occurring cysteines in the Zn-hook region (lanes 6, 8), and Mre11 remained unaffected under the crosslinking conditions as it has no cysteines. Next we assessed DNA end tethering by adding the DNA substrate after MR-2C was crosslinked in the presence of ATP (Fig 7D). Crosslinked MR-2C (lanes 6, 7) supported end ligation as well as non-crosslinked MR-2C (lanes 4, 5), and even promoted end ligation in the presence of closed circular competitor DNA (Supplementary Fig S5), similar to the R805E mutant, providing more evidence that the ATP-bound conformation binds with high specificity to DNA ends.

In contrast to the tethering assay, the MR-2C crosslinked complexes completely failed to resect DNA under oxidizing conditions (Fig 7E, lane 3). Notably, MR-2C was fully active in this assay under reducing conditions (lane 4): thus crosslinking of the head domains is responsible for activity loss in this resection assay. The 2C complexes were also tested in the plasmid resection assay with HerA-NurA, where it was clear that MR stimulation of HerA-NurA was abolished under oxidizing conditions but similar to WT under reducing conditions (Fig 7F, lanes 6, 7). WT MR also exhibited limited resection of the DNA substrate by itself, which is visible in the Southern blot (compare lanes 1 and 17), whereas MR-2C did not exhibit this activity under oxidizing conditions (lane 8), consistent with the absence of endonuclease activity with crosslinked MR-2C (Fig 7E). Importantly, ATP is still hydrolyzed by MR-2C when it is crosslinked (Supplementary Fig S5), thus opening from the ATP-bound state is required for MR endonuclease activity and promotion of long-range resection by HerA-NurA, consistent with SAXS data showing that the Mre11 active site is blocked by Rad50 in solution (Fig 1B) as well as crystallographic evidence (Lim *et al*, 2011; Mockel *et al*, 2011).

Rad50 ATP-driven movements regulate DSB repair *in vivo*

To comprehensively test the separation-of-function mutations, we examined the effects of the Rad50 mutations in *S. cerevisiae*, *S. pombe*, and *in vitro* signaling assays to develop an integrated functional model for ATP-induced conformational changes. First, we made I1214W and R1217E mutations in the *RAD50* gene of *S. cerevisiae*, (equivalent to the L802W and R805E mutations in *P. furiosus* Rad50). The Rad50 WT and mutant alleles were expressed under the control of the inducible *CUP1* promoter to normalize the expression levels (Supplementary Fig S6). These strains were exposed to camptothecin (CPT), which induces DNA strand breaks during replication by creating topoisomerase I covalent complexes. The strain expressing the I1214W mutant grew as well on CPT as the strain expressing WT protein, but the strain expressing the R1217E mutant grew very poorly on CPT, indicating an inability to repair endogenous DNA damage by homologous recombination (Fig 8A). Consistent with this phenotype, a defect in resection was also seen with the R1217E mutant in an assay for single-strand annealing which requires extensive resection (25 kb) for repair (Fig 8B). Lastly, we observed that resection of an HO endonuclease-induced break was rapid in *rad50* strains expressing the WT or I1214W alleles but that the strain expressing the R1217E allele was similar to the uncomplemented strain, again indicating a resection defect associated with R1217E (Supplementary Fig S6D).

We also examined non-homologous end joining in budding yeast, using two different assays. First, we used a chromosomal assay in which both precise and imprecise joining products can be quantitated (Palmbos *et al*, 2005; Supplementary Fig S6). Unlike the assay for CPT sensitivity, here both the R1217E and I1214W mutants showed a robust activity in promoting NHEJ, similar to the WT complemented strain (Fig 8C). Second, we used overexpression of the EcoRI restriction endonuclease to generate DSBs across the genome (Lewis *et al*, 1999). In this case the R1217E mutant improved the survival of the complemented *rad50* deletion strain significantly more than the WT or I1214W proteins, indicating a gain-of-function in this case where a massive DSB load has to be repaired for cell survival. Thus the R1217E mutant shows a separation-of-function such that the resection activities are specifically impaired but the end joining activities are intact and even hyperactive, consistent with the R805E Rad50 mutant results *in vitro*. The I1214W mutant shows nearly WT levels of function in all assays, similar to the Rad50 L802W mutant *in vitro* and consistent with the dominant role of homologous recombination in budding yeast repair of DNA double-strand breaks.

We also examined the equivalent *rad50* alleles in *S. pombe* to determine if the relationships between the ATP-driven switches are evolutionarily conserved in this organism. The I1192W, K1187E, and R1195E mutations were generated in the *rad50* gene of *S. pombe* (equivalent to the L802, R797 and R805 residues mutated in *P. furiosus* Rad50, respectively). The chromosomal *rad50*$^+$ locus was replaced with WT or mutant alleles encoding Rad50 with an N-terminal TAP-tag, and immunoblotting indicated that the mutations did not affect Rad50 abundance (Supplementary Fig S6). These mutants were exposed to ionizing radiation (IR) or CPT (Fig 8E). Similar to the *S. cerevisiae* results, the K1187E and R1195E mutants grew very poorly in the presence of DNA damaging agents (Williams *et al*, 2011) while the I1192W mutant displayed a phenotype intermediate between WT and the *rad50* strains.

To test the impact of Rad50 conformation on MRN signaling, we measured phosphorylation of histone H2A following IR to assess whether the *rad50* mutations impair the MRN-dependent function of

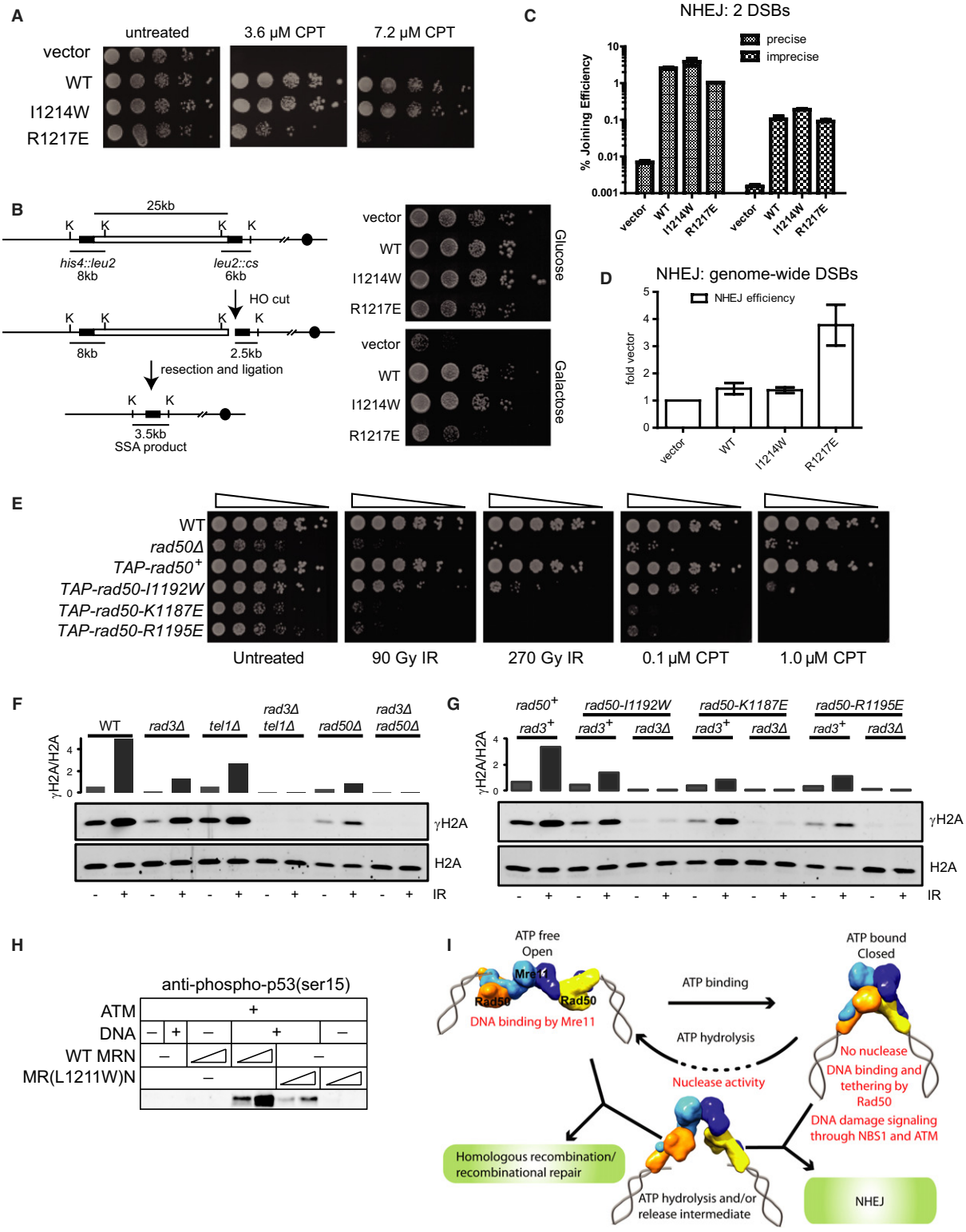

Tel1 (ATM). As both Tel1 and Rad3 (ATR) create phospho-H2A (γH2A; equivalent to γH2AX in metazoans) in *S. pombe* (Nakamura *et al*, 2004), these assays were performed in *rad3*$^{+}$ and *rad3Δ* backgrounds. We found that the large IR-induced increase in γH2A observed in WT was partially impaired in *tel1Δ* and *rad3Δ* single mutants and ablated in the double mutant (Fig 8F, G). The weak γH2A signal in the *rad50Δ* background was eliminated in the *rad50Δ rad3Δ* strain, supporting prior data establishing that MRN is

Figure 8. Rad50 separation-of-function mutations affect MRN DNA repair functions.

A *S. cerevisiae* survival assays with *rad50 S. cerevisiae* strains expressing vector only or WT, I1214W, or R1217E Rad50 proteins.

B Diagram of *S. cerevisiae* SSA assay (left)(Vaze *et al*, 2002). Survival of *rad50* S. cerevisiae strains expressing vector only or WT, I1214W, or R1217E Rad50 proteins before (glucose) or after (galactose) DSB induction at *leu2*::cs.

C Chromosomal NHEJ assay results with *S. cerevisiae* Rad50 variant strains, characterizing precise versus imprecise NHEJ-mediated joining events. See Supplementary Fig S6 for assay details. The average of 3 independent experiments is shown, with error bars indicating standard deviation.

D NHEJ assay with EcoRI induction, causing genome-wide DSBs. WT, I1214W, or R1217E alleles of Rad50 were expressed in a *rad50* strain and survival was measured after galactose induction of EcoRI for 8 hrs. The average of 5 independent experiments is shown, with the survival of each strain shown relative to the *rad50* strain that was normalized to 1; error bars indicate standard deviation.

E *S. pombe* survival assays of Rad50 variant strains.

F, G Western blots for γH2A and H2A levels in cell lysates after 90 Gy IR treatment of indicated *S. pombe* strains.

H Stimulation of ATM phosphorylation of p53 by the human MRN complex in vitro. Blots were probed with antibody against phospho-Ser15 of p53.

I Model of ATP-induced conformational changes in MR and the functions associated with each state. See text for details.

Source data are available online for this figure.

crucial for Tel1 signaling at DSBs (Lee & Paull, 2005; Nakada *et al*, 2003; You *et al*, 2005). Similar to *rad50Δ*, the *rad50-I1192W*, *-K1187E*, and *-R1195E* mutations all reduced γH2A in the *rad3*$^+$ background and nearly eliminated the γH2A signal in the *rad3Δ* background. Thus, mutations that impact ATP binding and turnover in Rad50 severely disrupt MRN functions in DNA repair and Tel1 (ATM) checkpoint signaling *in vivo*.

To further test the Rad50 mutations for effects on ATM activation, human MRN was expressed with R1214E and L1211W mutations (pfMR R805E and L802W equivalent, respectively), but we could only purify the L1211W variant. This complex exhibited severely reduced activity in stimulating ATM phosphorylation of p53 *in vitro* (Fig 8H), consistently indicating that the ATP-induced conformational changes in Rad50 and Mre11 are critical for ATM signaling of DNA damage.

Discussion

MR conformations control distinct pathway choices

In comprehensively examining how diverse and sometimes opposing MR activities are regulated by ATP and by Rad50 ABC-ATPase conformations, we found that MR complexes that are enhanced for the ATP-bound conformation show activities critical for DSB repair by end-joining pathways: reduced ATPase activity, reduced nuclease activities, stronger ATP binding, and more efficient binding and tethering of dsDNA ends. Conversely, MR complexes defective for stable ATP binding show activities critical for HR: increased ATPase activity, hyperactive endonuclease activity, and efficient end resection. These structure-based mutants achieve separation-of-function by deliberately altering Rad50 dynamics by shifting the relative stability of the nucleotide-induced conformational states with possible implications for other ABC-ATPases (Hopfner & Tainer, 2003).

These data suggest a model for ATP-induced conformational changes in MR and how they relate to MR biological functions (Fig 8I). In the 'open' conformation (Lammens *et al*, 2011), MR binds to DNA but is not-end-specific. When ATP binds to the catalytic domains, the complex transitions to the 'closed' state (Lim *et al*, 2011; Mockel *et al*, 2011; Williams *et al*, 2011); in this configuration MR binds DNA with specificity for ends, tethers DNA ends, promotes end ligation, and activates ATM (Lee *et al*, 2013), but cannot cleave DNA. We propose that release from the closed state that occurs with ATP hydrolysis generates an intermediate conformation that is competent for DNA end resection and collaboration with other enzymes that perform long-range resection. Finally, release of nucleotide returns the enzyme to the original open state.

Role of the Rad50 coiled-coil domain in catalytic domain dimers

Studies in budding yeast have shown that the coiled-coils are important for all biological functions of MRX, including HR, NHEJ and telomere maintenance (Hohl *et al*, 2011; Hopfner *et al*, 2002). Our results show that one distinct role of the coiled-coils is to mechanically connect the two catalytic domains of Rad50 and Mre11, leading to enhanced DNA end tethering. Addition of Mre11 to the Rad50 catalytic domains also recovers much of the DNA end tethering activity in the absence of the coiled-coils, so in this respect Mre11 dimerization and Rad50 association through the coils are reinforcing functions. Notably, the crosslinking experiments show that the isolated Rad50 catalytic domains do not interact in the absence of ATP, whereas in the full-length complex there is crosslinking in the absence of nucleotide that can be further stimulated by the addition of ATP. Thus, in the full-length complex the catalytic domains can sample the ATP-bound state without ATP, due to the coiled-coil linkage. Torsional strain applied through the coiled-coils may aid Mre11 dimer positioning into its active configuration, as proposed to explain how hook domain removal may alter the juxtaposition of ends within the globular domains (Hohl *et al*, 2011). Thus, full-length MR ATPase activity is higher than the Rad50 catalytic domains (a ~12-fold increase in k_{cat}), probably because their local concentration is increased by the dual connection imposed by Mre11 and the coiled-coil domains, a conclusion also supported by recent work showing that the coils promote ATM activation and Nbs1 binding to MR (Lee *et al*, 2013).

Regulation of Mre11 nuclease activity by Rad50

Previous results indicate that ATP binding by Rad50 alters Mre11 nuclease activity (Connelly & Leach, 1996; Herdendorf *et al*, 2011; Majka *et al*, 2012; Paull & Gellert, 1999; Trujillo & Sung, 2001). Here the mutant complexes and the site-specific crosslinking experiments show definitively that the closed state is incompatible with nuclease activity in magnesium conditions, in which the MR complex exhibits

5′ endonuclease activity as well as promoting the helicase and nuclease activities of the HerA/NurA complex. In contrast, release from the closed state (following ATP hydrolysis) promotes both Mre11 nuclease activity as well as HerA/NurA activity on linear DNA ends. These results agree generally with experiments performed with the *E. coli* SbcC/D complex, the T4 gp46/gp47 complex, and with the human MR complex (Herdendorf *et al*, 2011; Paull & Gellert, 1999; Trujillo & Sung, 2001), which showed that ATP is necessary for resection of dsDNA by MR. Lacking structural information about intermediates formed during hydrolysis, we postulate a transient state in which the Mre11 active site gains access to DNA that is inaccessible in the closed state (Fig 8I).

End tethering and the requirement for ATP

End-tethering assays revealed a surprising specificity for ATP over the non-hydrolyzable analogs ATPγS and AMP-PNP, despite the fact that both analogs induced conformational changes in Rad50 that resembled those induced by ATP (particularly ATPγS). This is not likely due to a requirement for ATP hydrolysis, since the R805E mutant promotes end tethering even better than the WT enzyme yet hydrolyzes ATP more slowly. It is possible that with the coiled-coils the conformation of MR when bound to ATP might be structurally distinct from that of the analog-bound complexes and that this difference could be important for the correct alignment of ends or access of other enzymes to the ends, even though it is not important for DNA binding by MR.

Surprisingly, L802W MR complex stimulates some ligation despite exhibiting a less stable 'closed' state. Yet, the L802W mutant in full-length form is closer to the WT enzyme characteristics than it is in Rad50cd form, and the short time that the L802W mutant spends in the closed state may be sufficient for ligation. Alternatively the opening of DNA helices by MR complexes (Cannon *et al*, 2013) may actually promote intermolecular association of DNA strands in an end tethering complex that survives even after the protein has returned to the open state. If so, a more rapid transition from closed to open state as seen with the L802W mutant would still be consistent with efficient end ligation.

Rad50 cavity and switch residues act as a communication hub

Structurally, the Rad50 cavity and arginine switches provide a communication hub between the two ATP binding sites of a single Rad50 subunit formed by the Walker A/B and signature motifs. They coordinate the conformational changes, and form an intricate communication network linking the signature motif to the catalytic step of the distal ATP binding site (through Walker B motif connections), and to the catalytic step of the other subunit through the D-loop and its connections to H855. This communication via the cavity is conceptually similar to the 'sectors' recently shown as important components of allosteric regulation to connect surface sites to active sites in dihydrofolate reductase (Reynolds *et al*, 2011).

We found that cavity mutations impair functions for archaeal, fission, budding yeast and human MR complexes; thus cavity regulated conformational plasticity may have key implications for evolution of distinct biological properties and regulation modes for Rad50 and other members of the ABC-ATPase superfamily, which includes mismatch repair ATPase MutS and ABC transporters (Hopfner & Tainer, 2003). Given segmentation of the ATP binding cassette into N- and C-terminal halves (Rad50) or assembled modular domains interacting *in trans* with effector domains (e.g. Cystic Fibrosis Transmembrane Conductance Regulator; CFTR, MalK transporters), cavities of varying size and composition may have evolved to define distinct emergent biological properties of the ATP binding cassette superfamily.

The well-characterized CFTR channel also undergoes a rotation in the ATPase domains upon ATP binding (Kirk & Wang, 2011). Interestingly, mapping of CFTR small-molecule potentiators that bind to its ABC-ATPase domain (Moran & Zegarra-Moran, 2005), such as genistein, identified three probable binding sites with the most likely (site 2) neighboring the arginine-switch and cavity regions found in Rad50. Coupling this information with our Rad50 results, showing cavity disruption alters the ABC-ATPase open versus closed states, suggests that such cavities are druggable; highlighting a key future challenge to design new small-molecules to effect biological outcomes controlled by Rad50 and ABC-ATPases that will have potential for both basic research and therapeutics.

Our results with the separation-of-function mutants *in vitro* plus the *S. cerevisiae and S. pombe in vivo* analyses suggest a molecular mechanism whereby MR complexes can concomitantly control what appears to be two opposing functions: DNA end bridging and resection. While our separation-of-function mutations act as permanent 'switches' to make malfunctioning MRN complexes, our results raise the possibility that during the DNA damage response, regulation of interacting partners and/or post-translational modification of the MRN complex may temporarily modulate its ATP binding and/or hydrolysis rates to control pathway outcomes. Indeed, several phosphorylation sites have been identified in Mre11 and Rad50 (Di Virgilio *et al*, 2009; Gatei *et al*, 2011), although effects on biochemical and biological outcomes have yet to be fully elucidated. It will be intriguing to investigate how such mechanisms may work to regulate MRN states and control replication fork stability, DSB repair and signaling in mammalian cells.

Materials and Methods

Plasmids and strains

See Supplementary materials for details.

Protein purification

Full-length and MRcd *P. furiosus* proteins were purified as described (Hopkins & Paull, 2008), as were the Rad50cd-linked and Rad50cd proteins (Williams *et al*, 2011). See Supplementary materials for details of gel filtration assays, protein crystallization, and SAXS determination. All recombinant proteins used in this work *in vitro* were derived from *P. furiosus*, with the exception of the human MRN complex used in Fig 8.

DNA binding assays

Gel mobility shift assays were performed as previously described (Lee *et al*, 2003), with modifications as described in Supplementary materials.

5′ resection assays

Assays shown in Figs 6A–C and 7E were performed as described (Hopkins & Paull, 2008) with 5 mM $MgCl_2$ and 1 mM ATP except with a fluorescent substrate (717 bp) made by PCR using primers TP2108/1621 with Cy3 on the 5′ end on the top strand. Assays in Fig 6B used TP2151 annealed to TP2109. For the assay in Fig 6D, the substrate consisted of TP74 annealed to TP124 (Paull & Gellert, 2000), with TP74 labeled with ^{32}P at the 5′ end. Reactions included 10 nM DNA substrate, 25 mM MOPS pH 7.0, 20 mM Tris pH 8.0, 1 mM $MnCl_2$, 8% glycerol, 80 mM NaCl, 2 mM DTT and 0.5 mM ATP at 65°C for 1 h. Reactions were stopped with 0.2% SDS and 10 mM EDTA, precipitated with ethanol, dried, dissolved in formamide, heated for 10 min at 100°C and separated on denaturing polyacrylamide gels (16 to 20%). After electrophoresis at 40 W for 2.5 h, gels with the TP2108/1621 and TP2151/2109 substrates were scanned in the Cy3 or Cy5 channel (Typhoon, GE). Gels with TP74/TP124 were dried and exposed to phosphorimager screens for analysis.

In reactions with HerA-NurA, 4 ng of PstI-digested pCDF1-b plasmid (0.16 nM) was incubated with MR and HerA-NurA at 65°C for 45 min with 25 mM MOPS pH 7.0, 20 mM Tris pH 8.0, 5 mM $MgCl_2$, 8% glycerol, 80 mM NaCl, 2 mM DTT and 0.5 mM ATP in a 10 μl reaction volume. The reactions were stopped by 0.2% SDS and 10 mM EDTA, separated by native agarose gel electrophoresis, stained with SYBR green (Invitrogen) and analyzed by phosphorimager (Typhoon, GE). The same gel was used for non-denaturing Southern analysis as described (Hopkins & Paull, 2008). A ^{32}P-radiolabeled RNA probe complementary to the 3′ strand was used to detect 5′-resected products, and the southern blot was analyzed by phosphorimager (GE).

DNA end tethering assay

The pCDF1-b plasmid was linearized with PstI to generate 4 nt 3′ overhangs. 10 μl ligation reactions contained 10 ng linearized DNA (0.4 nM) in the same buffer as for DNA binding except with 50 mM NaCl, with incubation at 65°C for 10 min with Mre11, Rad50, or MR complexes as indicated in figure legends. The temperature was then lowered to 16°C, and the reactions supplemented with *E. coli* DNA ligase buffer and 1,000 units *E. coli* DNA ligase (NAD-dependent, Fig 5) or with 10,000 units T4 DNA ligase (Fig 7). Reactions were further incubated at 16°C for 30 min and stopped by 0.2% SDS and 10 mM EDTA and incubated with 1 μg Proteinase K at 37°C for 45–60 min before separation by native gel electrophoresis, SYBR green staining, and phosphorimager analysis (Typhoon, GE). In Fig 5H, the substrate or competitor DNA (pCDF1-b, 0.2× or 0.5× the amount of substrate DNA) was added to the protein for 10 min before adding competitor or substrate, respectively and further incubation at 65°C for 10 min.

Crosslinking of ‘2C Rad50 complexes

Full-length MR-2C protein complexes were incubated at 65°C for 5 min with 25 mM MOPS pH 7.0, 20 mM Tris pH 8.0, 5 mM $MgCl_2$, 8% glycerol, 80 mM NaCl, 2 mM H_2O_2, 1 mM ATP, and 0.5 or 5 mM DTT as indicated. The crosslinked protein was diluted upon addition to the DNA end resection assay reactions (- DTT), reducing H_2O_2 concentration to 0.4 mM and DTT to 0.2 mM or 2 mM. Rad50cd-2C proteins were crosslinked by incubation of 3.5 μM protein in 25 mM MOPS pH 7.0, 5 mM $MgCl_2$, 120 mM NaCl and 0.5 mM ATP or 2 mM AMP/ADP/ATPγS/Ap5A without H_2O_2.

Partial proteolysis

Rad50 or MR proteins were incubated with nucleotides at 65°C for 10 min. 0.2 μg trypsin (Promega) was added and incubated at 37°C for 2 h (or 16 h in Fig 3C). The digestion products were resolved by SDS–PAGE stained with Coomassie. For N-terminal sequencing, proteins were transferred to PVDF membrane and stained by Coomassie. The molecular mass was determined by ESI mass spectrometry analysis of the tryptic digests: Rad50cd (5 μg) was incubated in a buffer containing 25 mM MOPS pH 7.0, 20 mM Tris pH 8.0, 5 mM $MgCl_2$, 8% glycerol, 80 mM NaCl, 2 mM DTT, and nucleotides as indicated (0.5 mM), in a volume of 10 μl at 65°C for 10 min. The reactions were cooled to 25°C for 5 min, 0.2 μg trypsin (Promega) was added and incubated at 37°C for 2 h (or 16 h in Fig 3C).

N-terminal sequencing

Automated Edman-based N-terminal sequencing was performed using a Procise 492cLc Protein Sequencer (Applied Biosystems) using standard cycles for PVDF membrane analysis.

ATP hydrolysis and kinetic studies

ATP hydrolysis was measured at 65°C as described (Bhaskara *et al*, 2007). Values shown in Fig 4C were calculated using non-linear regression analysis with Graphad Prism. See also Supplementary Fig S4.

ATP binding with TNP-ATP

10 μl reactions contained 200 nM MR with 0–200 μM TNP-ATP [2′,3′-*O*-(2,4,6-Trinitrophenyl)adenosine-5′-triphosphate] and 25 mM MOPS pH 7.0, 20 mM Tris pH 8.0, 5 mM $MgCl_2$, 8% glycerol, 80 mM NaCl, 2 mM DTT in a 1,536-well plate (Corning, #3728). Fluorescence emission spectra were recorded with a Safire^2 plate reader (Tecan) using 290 nm excitation for Trp. The quenching of Trp emission at 330 nm is presented as a Stern-Volmer plot F_0/F versus [TNP-ATP], where F_0 and F are the fluorescence intensities in the absence and presence of quencher.

S. cerevisiae NHEJ assays

S. cerevisiae strains are listed in Supplementary Table S3. The *rad50* strain TP3619 was used for the chromsomal NHEJ assay, essentially as previously described (Palmbos *et al*, 2005). The *rad50* strain KRY78 was used for the EcoRI NHEJ assay, as previously described (Lewis *et al*, 1999). Modifications and further details are in Supplementary materials.

S. cerevisiae SSA assay

The assay was performed essentially as described (Vaze *et al*, 2002) with modifications in Supplementary materials.

S. cerevisiae resection assay

The assay was performed as described (Moncalian *et al*, 2004) with modifications in Supplementary materials.

S. pombe DNA damage sensitivity assays and H2A phosphorylation assay

S. pombe strains were manipulated by standard techniques (Forsburg & Rhind, 2006) with strains listed in Supplementary Table S2 and details of growth and signaling assays in Supplementary materials.

In vitro kinase assays

MRN complexes and dimeric ATM were purified as described (Bhaskara *et al*, 2007; Lee & Paull, 2006). ATM kinase assays contained 50 mM HEPES, pH 7.5, 50 mM KCl, 5 mM $MgCl_2$, 10% glycerol, 1 mM ATP, and 1 mM DTT and were performed for 90 min at 30°C in 40 μl as described (Lee & Paull, 2006). See Supplementary materials for details.

Accession codes

Coordinates and structure factors of the four Rad50 mutant structures detailed in this manuscript have been deposited in the protein databank and have the following PDB codes: 4NCH (L802W), 4NCI (R805E), 4NCJ (R805E + ADP/BeF), and 4NCK (R797G).

Supplementary information for this article is available online: http://emboj.embopress.org

Acknowledgments

We thank members of the Paull, Tainer, and Russell laboratories for comments, Christophe Redon for the γH2A antibody, Antony Carr for the TAP-Rad50 *S. pombe* strain, and Tom Wilson, Jim Haber, Sang Eun Lee, and Tom Petes for *S. cerevisiae* strains. This study was supported by NIH grants CA094008 to T.P., CA092584 to J.T. and T.P., CA117638 to J.T. and P.R., CA077325 to P.R., and intramural research program of the US National Institutes of Health (NIH), National Institute of Environmental Health Sciences (NIEHS) (1Z01ES102765-01) to R.S.W. The SIBYLS beamline (BL12.3.1) at the Advanced Light Source is supported by United States Department of Energy program Integrated Diffraction Analysis Technologies and NIH MINOS R01GM105404. Mass spectroscopy was performed by the Protein and Metabolite Analysis Facility at UT Austin.

Author contributions

RAD, GJW, and RSW generated reagents, designed and performed experiments, interpreted results, and helped to write the manuscript. OL and J-HL generated reagents and performed and analyzed experiments. JK, SC, and GG generated reagents and contributed to the experiments. PR, JAT, and TTP helped to design and interpret experiments and edited the manuscript.

Conflict of interest

The authors declare that they have no conflict of interest.

References

Alani E, Padmore R, Kleckner N (1990) Analysis of WT and rad50 mutants of yeast suggests an intimate relationship between meiotic chromosome synapsis and recombination. *Cell* 61: 419 – 436

Bhaskara V, Dupre A, Lengsfeld B, Hopkins BB, Chan A, Lee JH, Zhang X, Gautier J, Zakian VA, Paull TT (2007) Rad50 adenylate kinase activity regulates DNA tethering by Mre11/Rad50 complexes. *Mol Cell* 25: 647 – 661

Cannon B, Kuhnlein J, Yang SH, Cheng A, Schindler D, Stark JM, Russell R, Paull TT (2013) Visualization of local DNA unwinding by MRN using single-molecule FRET. *Proc Natl Acad Sci U S A* 110: 18868 – 18873

Chen L, Trujillo KM, Van Komen S, Roh DH, Krejci L, Lewis LK, Resnick MA, Sung P, Tomkinson AE (2005) Effect of amino acid substitutions in the rad50 ATP binding domain on DNA double strand break repair in yeast. *J Biol Chem* 280: 2620 – 2627

Connelly JC, Leach DR (1996) The sbcC and sbcD genes of *Escherichia coli* encode a nuclease involved in palindrome inviability and genetic recombination. *Genes Cells* 1: 285 – 291

Di Virgilio M, Ying CY, Gautier J (2009) PIKK-dependent phosphorylation of Mre11 induces MRN complex inactivation by disassembly from chromatin. *DNA Repair* 8: 1311 – 1320

Doksani Y, Bermejo R, Fiorani S, Haber JE, Foiani M (2009) Replicon dynamics, dormant origin firing, and terminal fork integrity after double-strand break formation. *Cell* 137: 247 – 258

Forsburg SL, Rhind N (2006) Basic methods for fission yeast. *Yeast* 23: 173 – 183

Gatei M, Jakob B, Chen P, Kijas AW, Becherel OJ, Gueven N, Birrell G, Lee JH, Paull TT, Lerenthal Y, Fazry S, Taucher-Scholz G, Kalb R, Schindler D, Waltes R, Dork T, Lavin MF (2011) ATM protein-dependent phosphorylation of Rad50 protein regulates DNA repair and cell cycle control. *J Biol Chem* 286: 31542 – 31556

Herdendorf TJ, Albrecht DW, Benkovic SJ, Nelson SW (2011) Biochemical characterization of bacteriophage T4 Mre11-Rad50 complex. *J Biol Chem* 286: 2382 – 2392

Hiratsuka T (1976) Fluorescence properties of 2′ (or 3′)-O-(2,4,6-trinitrophenyl) adenosine 5′-triphosphate and its use in the study of binding to heavy meromyosin ATPase. *Biochim Biophys Acta* 453: 293 – 297

Hohl M, Kwon Y, Galvan SM, Xue X, Tous C, Aguilera A, Sung P, Petrini JH (2011) The Rad50 coiled-coil domain is indispensable for Mre11 complex functions. *Nat Struct Mol Biol* 18: 1124 – 1131

Hopfner KP, Craig L, Moncalian G, Zinkel RA, Usui T, Owen BA, Karcher A, Henderson B, Bodmer JL, McMurray CT, Carney JP, Petrini JH, Tainer JA (2002) The Rad50 zinc-hook is a structure joining Mre11 complexes in DNA recombination and repair. *Nature* 418: 562 – 566

Hopfner KP, Karcher A, Shin DS, Craig L, Arthur LM, Carney JP, Tainer JA (2000) Structural biology of Rad50 ATPase: ATP-driven conformational control in DNA double-strand break repair and the ABC-ATPase superfamily. *Cell* 101: 789 – 800

Hopfner KP, Tainer JA (2003) Rad50/SMC proteins and ABC transporters: unifying concepts from high-resolution structures. *Curr Opin Struct Biol* 13: 249 – 255

Hopkins B, Paull TT (2008) The *P. furiosus* Mre11/Rad50 complex promotes 5′ strand resection at a DNA double-strand break. *Cell* 135: 250 – 260

Hura GL, Budworth H, Dyer KN, Rambo RP, Hammel M, McMurray CT, Tainer JA (2013) Comprehensive macromolecular conformations mapped by quantitative SAXS analyses. *Nat Methods* 10: 453 – 454

de Jager M, van Noort J, van Gent DC, Dekker C, Kanaar R, Wyman C (2001) Human Rad50/Mre11 is a flexible complex that can tether DNA ends. *Mol Cell* 8: 1129 – 1135

Kirk KL, Wang W (2011) A unified view of cystic fibrosis transmembrane conductance regulator (CFTR) gating: combining the allosterism of a ligand-gated channel with the enzymatic activity of an ATP-binding cassette (ABC) transporter. *J Biol Chem* 286: 12813 – 12819

Krogh BO, Symington LS (2004) Recombination proteins in yeast. *Annu Rev Genet* 38: 233 – 271

Lamarche BJ, Orazio NI, Weitzman MD (2010) The MRN complex in double-strand break repair and telomere maintenance. *FEBS Lett* 584: 3682 – 3695

Lammens K, Bemeleit DJ, Mockel C, Clausing E, Schele A, Hartung S, Schiller CB, Lucas M, Angermuller C, Soding J, Strasser K, Hopfner KP (2011) The Mre11:Rad50 structure shows an ATP-dependent molecular clamp in DNA double-strand break repair. *Cell* 145: 54 – 66

Lee J-H, Ghirlando R, Bhaskara V, Hoffmeyer MR, Gu J, Paull TT (2003) Regulation of Mre11/Rad50 by Nbs1: effects on nucleotide-dependent DNA binding and association with ATLD mutant complexes. *J Biol Chem* 278: 45171 – 45181

Lee JH, Mand MR, Deshpande RA, Kinoshita E, Yang SH, Wyman C, Paull TT (2013) Ataxia Telangiectasia-Mutated (ATM) kinase activity is regulated by ATP-driven conformational changes in the Mre11/Rad50/Nbs1 (MRN) Complex. *J Biol Chem* 288: 12840 – 12851

Lee JH, Paull TT (2005) ATM activation by DNA double-strand breaks through the Mre11-Rad50-Nbs1 complex. *Science* 308: 551 – 554

Lee JH, Paull TT (2006) Purification and biochemical characterization of ataxia-telangiectasia mutated and Mre11/Rad50/Nbs1. *Methods Enzymol* 408: 529 – 539

Lee JH, Paull TT (2007) Activation and regulation of ATM kinase activity in response to DNA double-strand breaks. *Oncogene* 26: 7741 – 7748

Lewis LK, Westmoreland JW, Resnick MA (1999) Repair of endonuclease-induced double-strand breaks in Saccharomyces cerevisiae: essential role for genes associated with nonhomologous end- joining. *Genetics* 152: 1513 – 1529

Lim HS, Kim JS, Park YB, Gwon GH, Cho Y (2011) Crystal structure of the Mre11-Rad50-ATPgammaS complex: understanding the interplay between Mre11 and Rad50. *Genes Dev* 25: 1091 – 1104

Majka J, Alford B, Ausio J, Finn RM, McMurray CT (2012) ATP hydrolysis by RAD50 protein switches MRE11 enzyme from endonuclease to exonuclease. *J Biol Chem* 287: 2328 – 2341

Mockel C, Lammens K, Schele A, Hopfner KP (2011) ATP driven structural changes of the bacterial Mre11:Rad50 catalytic head complex. *Nucleic Acids Res* 40: 914 – 927

Moncalian G, Lengsfeld B, Bhaskara V, Hopfner KP, Karcher A, Alden E, Tainer JA, Paull TT (2004) The rad50 signature motif: essential to ATP binding and biological function. *J Mol Biol* 335: 937 – 951

Moran O, Zegarra-Moran O (2005) A quantitative description of the activation and inhibition of CFTR by potentiators: Genistein. *FEBS Lett* 579: 3979 – 3983

Nakada D, Matsumoto K, Sugimoto K (2003) ATM-related Tel1 associates with double-strand breaks through an Xrs2-dependent mechanism. *Genes Dev* 17: 1957 – 1962

Nakamura TM, Du LL, Redon C, Russell P (2004) Histone H2A phosphorylation controls Crb2 recruitment at DNA breaks, maintains checkpoint arrest, and influences DNA repair in fission yeast. *Mol Cell Biol* 24: 6215 – 6230

Oldham ML, Khare D, Quiocho FA, Davidson AL, Chen J (2007) Crystal structure of a catalytic intermediate of the maltose transporter. *Nature* 450: 515 – 521

Palmbos PL, Daley JM, Wilson TE (2005) Mutations of the Yku80 C terminus and Xrs2 FHA domain specifically block yeast nonhomologous end joining. *Mol Cell Biol* 25: 10782 – 10790

Paull TT, Gellert M (1998) The 3′ to 5′ exonuclease activity of Mre 11 facilitates repair of DNA double-strand breaks. *Mol Cell* 1: 969 – 979

Paull TT, Gellert M (1999) Nbs1 potentiates ATP-driven DNA unwinding and endonuclease cleavage by the Mre11/Rad50 complex. *Genes Dev* 13: 1276 – 1288

Paull TT, Gellert M (2000) A mechanistic basis for Mre11-directed DNA joining at microhomologies. *Proc Natl Acad Sci U S A* 97: 6409 – 6414

Putnam CD, Hammel M, Hura GL, Tainer JA (2007) X-ray solution scattering (SAXS) combined with crystallography and computation: defining accurate macromolecular structures, conformations and assemblies in solution. *Q Rev Biophys* 40: 191 – 285

Rambo RP, Tainer JA (2011) Characterizing flexible and intrinsically unstructured biological macromolecules by SAS using the Porod-Debye law. *Biopolymers* 95: 559 – 571

Rambo RP, Tainer JA (2013a) Accurate assessment of mass, models and resolution by small-angle scattering. *Nature* 496: 477 – 481

Rambo RP, Tainer JA (2013b) Super-resolution in solution X-ray scattering and its applications to structural systems biology. *Annu Rev Biophys* 42: 415 – 441

Reynolds KA, McLaughlin RN, Ranganathan R (2011) Hot spots for allosteric regulation on protein surfaces. *Cell* 147: 1564 – 1575

Schlacher K, Christ N, Siaud N, Egashira A, Wu H, Jasin M (2011) Double-strand break repair-independent role for BRCA2 in blocking stalled replication fork degradation by MRE11. *Cell* 145: 529 – 542

Stracker TH, Petrini JH (2011) The MRE11 complex: starting from the ends. *Nat Rev Mol Cell Biol* 12: 90 – 103

Tittel-Elmer M, Alabert C, Pasero P, Cobb JA (2009) The MRX complex stabilizes the replisome independently of the S phase checkpoint during replication stress. *EMBO J* 28: 1142 – 1156

Trujillo KM, Sung P (2001) DNA structure-specific nuclease activities in the Saccharomyces cerevisiae Rad50/Mre11 complex. *J Biol Chem* 13: 13

Vaze MB, Pellicioli A, Lee SE, Ira G, Liberi G, Arbel-Eden A, Foiani M, Haber JE (2002) Recovery from checkpoint-mediated arrest after repair of a double-strand break requires Srs2 helicase. *Mol Cell* 10: 373 – 385

Williams GJ, Williams RS, Williams JS, Moncalian G, Arvai AS, Limbo O, Guenther G, SilDas S, Hammel M, Russell P, Tainer JA (2011) ABC ATPase signature helices in Rad50 link nucleotide state to Mre11 interface for DNA repair. *Nat Struct Mol Biol* 18: 423 – 431

Williams RS, Dodson GE, Limbo O, Yamada Y, Williams JS, Guenther G, Classen S, Glover JN, Iwasaki H, Russell P, Tainer JA (2009) Nbs1 flexibly tethers Ctp1 and Mre11-Rad50 to coordinate DNA double-strand break processing and repair. *Cell* 139: 87 – 99

Williams RS, Moncalian G, Williams JS, Yamada Y, Limbo O, Shin DS, Groocock LM, Cahill D, Hitomi C, Guenther G, Moiani D, Carney JP, Russell P, Tainer JA (2008) Mre11 dimers coordinate DNA end bridging and nuclease processing in double-strand-break repair. *Cell* 135: 97 – 109

Williams RS, Williams JS, Tainer JA (2007) Mre11-Rad50-Nbs1 is a keystone complex connecting DNA repair machinery, double-strand break signaling, and the chromatin template. *Biochem Cell Biol* 85: 509 – 520

You Z, Chahwan C, Bailis J, Hunter T, Russell P (2005) ATM activation and its recruitment to damaged DNA require binding to the C terminus of Nbs1. *Mol Cell Biol* 25: 5363 – 5379

